International Journal of Applied Earth Observation and Geoinformation 26 (2014) 270–285

Contents lists available at ScienceDirect

International Journal of Applied Earth Observation and Geoinformation

journal homepage: www.elsevier.com/locate/jag

First results of the earth observation Water Cycle Multi-mission Observation Strategy (WACMOS)

Z. Su [a,*], D. Fernández-Prieto [b], J. Timmermans [a], X. Chen [a], K. Hungershoefer [c], R. Roebeling [d,e], M. Schröder [c], J. Schulz [e,c], P. Stammes [e], P. Wang [e], E. Wolters [e]

[a] Faculty of Geo-Information Science and Earth Observation (ITC), University of Twente, Enschede, The Netherlands
[b] European Space Agency, ESRIN, Frascati, Italy
[c] Deutscher Wetterdienst, Satellite Application Facility on Climate Monitoring, Dept. Climate and Environment, Offenbach, Germany
[d] Royal Netherlands Meteorological Institute (KNMI), The Netherlands
[e] European Organisation for the Exploitation of Meteorological Satellites (EUMETSAT), Darmstadt, Germany

ARTICLE INFO

Article history:
Received 24 February 2013
Accepted 9 August 2013

Keywords:
Earth observation
Evapotranspiration
Solar irradiance
Precipitation
Water vapour

ABSTRACT

Observing and monitoring the different components of the global water cycle and their dynamics are essential steps to understand the climate of the Earth, forecast the weather, predict natural disasters like floods and droughts, and improve water resources management. Earth observation technology is a unique tool to provide a global understanding of many of the essential variables governing the water cycle and monitor their evolution from global to basin scales. In the coming years, an increasing number of Earth observation missions will provide an unprecedented capacity to quantify several of these variables on a routine basis. However, this growing observational capacity is also increasing the need for dedicated research efforts aimed at exploring the potential offered by the synergies among different and complementary EO data records. In this context, the European Space Agency (ESA) launched the Water Cycle Multi-mission Observation Strategy (WACMOS) in 2009 aiming at enhancing, developing and validating a novel set of multi-mission based methods and algorithms to retrieve a number of key variables relevant to the water cycle. In particular the project addressed four major scientific challenges associated to a number of key variables governing the water cycle: evapotranspiration, soil moisture, cloud properties related to surface solar irradiance and precipitation, and water vapour. This paper provides an overview of the scientific results and findings with the ultimate goal of demonstrating the potential of strategies based on utilizing multi-mission observations in maximizing the synergistic use of the different types of information provided by the currently available observation systems and establish the basis for further work.

Contents

* Corresponding author.
E-mail address: z.su@utwente.nl (Z. Su).

0303-2434
http://dx.doi.org/10.1016/j.jag.2013.08.002

1. Introduction

The water cycle is a complex process driven by solar radiation. The evaporation of water from open water, bare soil and wet surfaces is controlled by energy and water availability and near-surface atmospheric conditions (air temperature, humidity and wind-speed), while transpiration of water is also controlled by plants. The result of evaporation and transpiration is the presence of water vapour in the atmosphere, a prerequisite for cloud formation. If cloud condensation nuclei are present and if the atmospheric state allows for condensation, clouds are formed which are then globally distributed by winds. In the presence of precipitating clouds, water returns back to the Earth's surface in the form of precipitation. Surface water may also infiltrate into the soil, moistening the soil layers and accumulating as groundwater replenishing aquifers. Aquifers can store water for several years, provide water for human activities, or discharge it naturally to the surface or to the oceans. The response of the hydrological cycle to global warming is expected to be far reaching (Bengtsson, 2010). Because different physical processes control the changes in water vapour, evaporation and precipitation, a more extreme distribution of precipitation is expected leading to, in general, wet regions getting wetter and dry ones becoming dryer. As such the changes in the hydrological cycle as a consequence of climate warming may be more severe than the temperature changes, due primarily to large increases in extreme precipitation rates (Lenderink and van Meijgaard, 2010).

In this context, it is essential to accurately observe long-term dynamics of the key variables which governs water cycle processes from global to local scale. This observational information can be used not only to analyze the spatial and temporal variability in the key components of the water cycle, but also to further understand the energy and water cycle interactions between land and atmosphere, which may influence climate variability. Such global and continuous observations can only be secured by the effective use of Earth Observation (EO) satellites as a major complement to in-situ observation networks.

In recent years, EO technology has proved to be a major source of data to retrieve an increasing number of hydro-climatic variables, including radiation and cloud properties (Jacobowitz et al., 2003; Zhang et al., 2004; Schulz et al., 2009), precipitation (Kummerow et al., 2001; Huffman et al., 2001; Kidd and Levizzani, 2011), evapotranspiration (Kalma et al., 2008; Jiménez et al., 2011), soil moisture (Aires and Prigent, 2006; de Jeu et al., 2008), water vapour (Randal et al., 1996; Schulz et al., 2009), and many others (see for example, GEO, 2005; ESA, 2006; CEOS, 2009; Su et al., 2010,2011). Such measurements not only have enhanced our capabilities to predict in a reliable manner the variations in the global energy and water cycle but also have provided a key contribution to the improvement of water governance, the mitigation of water-related natural hazards and the sustainable human development (GEO, 2007; IPCC, 2008).

Despite the availability of abundant satellite data for the assessment of different components of the water cycle, water budget closure at the scale of even large continental river basins is currently not possible on the basis of satellite data alone (Gao et al., 2010). In the coming years, an increasing number of EO missions will provide unprecedented possibilities to observe the Earth's surface, its interior and the atmosphere, opening a new era in EO and water cycle science, and therefore also in hydrology and water resources management. As examples, the Soil Moisture and Ocean Salinity (SMOS) mission (Kerr et al., 2010) for retrieving soil moisture and ocean salinity information was launched in November 2009 and the Aquarius satellite (http://aquarius.nasa.gov/) for ocean salinity was launched in June 2011. Next the Soil Moisture Active and Passive mission (SMAP) (Entekhabi et al., 2010) is planned for launch in 2014–2015 for providing global maps of soil moisture and surface freeze/thaw state. Other planned missions include the Surface Water and Ocean Topography (SWOT) (http://swot.jpl.nasa.gov/), the Global Precipitation Measurement (GPM) mission (http://gpm.gsfc.nasa.gov/), the Gravity Recovery and Climate Experiment (GRACE) follow-on mission (http://esto.nasa.gov/news/news_gracefollowon.html), the ESA's EarthCARE mission (ESA, 2004; http://www.esa.int/esaLP/ASESMYNW9SC_LPearthcare_0.html) for improving the representation and understanding of the Earth's radiative balance in climate and numerical weather prediction models, as well as the planned operational Sentinel satellites (http://www.esa.int/Our_Activities/Observing_the_Earth/GMES/). This growing observational capacity is also increasing the need for dedicated research efforts aimed at exploring the potential for the synergistic exploitation of the different and complementary capacities offered by existing EO data records and new sensors.

In this context, the European Space Agency (ESA) launched the Water Cycle Multi-Mission Observation Strategy (WACMOS) aimed at contributing to existing efforts to enhance, develop and validate a novel set of multi-mission based methods and algorithms to retrieve a number of key variables relevant to the water cycle. In particular, four main scientific challenges and observational gaps have been addressed:

- Advancing towards the development of a global high resolution evapotranspiration product;
- Advancing towards a 30-year consistent data record of surface soil moisture information by merging existing passive and active microwave data sets;
- Exploring the synergies between geostationary and polar orbiting satellites to derive cloud properties related to surface solar irradiance and precipitation;
- Exploring the synergies between geostationary and polar orbiting satellite data sets to enhance current water vapour products.

This paper provides an overview of the different methods, algorithms and products developed with a focus on the atmospheric part of the water cycle components. Technical descriptions about the soil moisture products have been reported by Dorigo et al. (2010) and Liu et al. (2011).

2. Background and WACMOS products

Table 1 presents a list of WACMOS products, their descriptions, the used sensors, areas of coverage, spatial and temporal resolutions, and accuracy and precision. Backgrounds for the choices of methodologies and products are given in the following separately.

Table 1
Overview of WACMOS product properties. Codes for temporal resolution are: I = instantaneous, H1 = hourly value, D = daily mean and M = monthly mean. Codes for areas are: MD = MSG disc and GC = global coverage. Codes for resolution are: HR = high resolution, LR = low resolution.

Product group	Product name	Sensor	Accuracy (precision)	Area	Spatial and temporal resolution	Unit
Evapotranspiration	ET	AATSR, MERIS, MODIS	25% (uncertainty on land/ocean) 25% (uncertainty on land/ocean)	GC	1 km × 1 km, and 25 km × 25 km	mm
Soil moisture	SOILM	AMSR-E, Windsat, TRMM, SSM/I, SMMR, ERS 1-2, ASCAT	0.04–0.08 depending on land cover (variable)	GC	0.25° grid, D	$m^3\ m^{-3}$
Clouds	SSI SSI PRECIP	SEVIRI SCIAMACHY SEVIRI	3(25)D 10(75)1 0.1(1.0)1	MD GC MD	3 km × 3 km,1,D,M 30 km × 60 km,1 3 km × 3 km,1,D,M	$W\ m^{-2} W\ m^{-2}$ $mm\ h^{-1}$
Water Vapour	wv	SEVIRI+IASI	0.2 (0.8), 0.6 (2.0), 0.8 (3.0) (for top, middle and bottom layer)	MD	$(0.25°)^2$, 3H	$kg\ m^{-2}$
	wv	SEVIRI+MERIS	1(4)	NEEur.	$(0.025°)^2$, 3H	$kg\ m^{-2}$

2.1. Evapotranspiration

Evapotranspiration (ET) is the process in which water is transferred from the surface to the atmosphere (Kalma et al., 2008) as a combination of soil and water evaporation and vegetation transpiration. While evaporation is only controlled by the physical processes of diffusion and convection, transpiration is also controlled by biological process, like photosynthesis.

Evapotranspiration provides the link between energy balances, water budgets and plant growth and plays a vital role in the energy cycle, the water cycle and the carbon cycle (Bowen, 1926; Penman, 1948; Monteith, 1965). By returning available water from the surface to the atmosphere, terrestrial evapotranspiration regulates the biological environment and its water use efficiency. In addition, evapotranspiration is a key quantity for the estimation of crop yield, irrigation water management, drought assessment, fire susceptibility, convective precipitation patterns as well as catchment water budgets. All these applications ideally require an evapotranspiration product with higher spatial-temporal resolution than currently available.

Over the last couple of years several initiatives, such as the LandFLUX Initiative (Jiménez et al., 2011; Mueller et al., 2011), have aimed to evaluate and develop large scale evapotranspiration products. In general these products can be divided into four groups: field measurement upscaling methods, land surface models, reference methods and energy balance methods. The field measurement upscaling methods use actual measurements from the field to estimate evapotranspiration in initiatives like Fluxnet (Baldocchi et al., 2001). As these measurements in general have a too small footprint for global application upscaling is aided by using satellite observations (Jung et al., 2010). The disadvantage of these methods is that the spatial resolution (0.5°) provided is still too coarse for most hydrological applications. Land surface models, like those adopted in the European Centre for Medium-range Weather Forecasts reanalysis (ECMWF ERA-interim) (Dee et al., 2011) and the Global Land Data Assimilation System (GLDAS) (Rodell et al., 2004), use routine measurements of meteorological variables to simulate the land surface processes. These models in general do not use surface remote sensing data for forcing, and have a coarse resolution (>1.0°). Recently the European Organisation for the Exploitation of Meteorological Satellites (EUMETSAT) Satellite Application Facility on Land Surface Analysis (LandSAF) has incorporated METEOSAT Second Generation (MSG) data into the ECMWF TESSEL model (Balsamo et al., 2009; Ghilain et al., 2011). While the resolution has greatly increased, the data products are restricted to the MSG disc area. Reference methods (Mu et al., 2007; Fisher et al., 2008) rely on the calculation of a potential or reference evapotranspiration and combining this with crop or environmental coefficients (Miralles et al., 2011) to derive actual evapotranspiration. Energy balance methods attempt to quantify the actual processes on the land surface (e.g. Su, 2002). Several studies (McCabe and Wood, 2006; Jiménez et al., 2011; Mueller et al., 2011; Vinukollu et al., 2011) have been performed to investigate the performance of energy balance algorithms, like the Surface Energy Balance System (SEBS) (Su, 2002), the Two Source Energy Balance (TSEB) and ALEXI (Anderson et al., 2007). Recently a global evapotranspiration product from 2002–2006 using SEBS and MODIS data has been made available (Vinukollu et al., 2011) and Table 2 summarises some available satellite based evapotranspiration products (per. Comm. M. McCabe).

The Surface Energy Balance System (SEBS) (Su, 2002) circumvents problems of local calibration, by using physical parameterization (Su et al., 2001) of the turbulent heat fluxes for different states of the land surface and the atmosphere based on the similarity theory (Obukhov, 1971; Brutsaert, 1999). For this reason we use SEBS in WACMOS as the baseline algorithm. The algorithm uses three sets of input parameters and variables that can either be measured using remote sensing sensors (e.g. albedo, emissivity, land surface temperature and leaf area index (LAI)) with high spatial resolution and obtained from mesoscale atmospheric models (wind speed, air temperature and humidity, and incoming short and long wave radiation) with lower spatial resolution. Since land surface temperature represents the thermal dynamic states of the surface, use of it in estimation of evapotranspiration utilises direct information related surface radiative forcing, thermal dynamic processes and water stress of the concerned surface, which are most relevant to the processes involved in evapotranspiration.

Sensors such as the Advanced Along Track Scanning Radiometer (AATSR) and the Medium Resolution Imaging Spectrometer (MERIS) sensors onboard the Environmental Satellite (ENVISAT) fit the spatio-temporal requirement of the evapotranspiration product; AATSR provides high resolution accurate land and ocean surface temperature measurements and MERIS provides high resolution optical measurements (needed for estimating albedo and LAI). Using data from these polar orbiting satellite instruments restricts the temporal resolution of the final product, as the revisit time is longer than a single day. The incorporation of data from geostationary satellites could solve this problem and additionally capture the diurnal pattern of evaporative fraction. However this has not been performed currently due to the high

Table 2
Available satellite based evapotranspiration products (Source: M. McCabe) (PM: Penman-Monteith1; PT: Priestly-Taylor; MOST: Monin-Obkuhov Similarity Theory; SEBS: Surface Energy Balance System; PML: Penman-Monteith with Leuning physiological parameters).

Product	Theoretical basis	Spatial resolution	Temporal resolution	Temporal coverage	References
UMONT-A (University of Montana)	PM	1 km	8-day	2000–2010	Zhang et al., 2010a, 2009
UMONT-B (University of Montana)	PM	8 km	Daily	1983–2006	Mu et al., 2009, 2007
CSIRO-PML (CSIRO)	PM	0.5°	Monthly	1981–2006	Leuning et al., 2008; Zhang et al., 2010b,c
PRU-PM (Princeton University – PM)	PM	l°–2°	3 h/Daily	1984–2007	Sheffield et al., 2010; Mu et al., 2007; Ferguson et al., 2010; Vinukollu et al., 2011
PRU-SEBS (Princeton University – SEBS)	MOST/SEBS	5 km	3 h/Daily	2000–2010	Ferguson et al., 2010; Vinukollu et al., 2011
PRU-PT (Princeton University – PT)	PT	l°–2°	3 h/Daily	1984–2007	Ferguson et al., 2010; Vinukollu et al., 2011
UCB-JPL (University of California Berkeley)	PT	1 km—1°	Monthly	1984–2010	Fisher et al., 2008, 2011
GLEAM (Vrije Universiteit Amsterdam)	PT	0.25°	Daily	1984–2007	Miralles et al., 2010, 2011
ALEXI (United States Department of Agriculture)	MOST/Two-source	0.25°	Daily	2000–2010	Anderson et al., 2007, 2008
UMT/BNU (University of Maryland/Texas/Beij ing Normal University)	Empirical-PM	1°	Daily	1982–2006	Wang et al., 2007, 2010a,b
Observatoire de Paris	Neural Network	0.5°	Monthly	1992–1999	Jiménez et al. (2009)
Max-Planck Institute for Biogeochemistry	Tree-ensemble	0.25°	Monthly	1982–2008	Jung et al., 2009, 2010

computational demands. Therefore the final product still contains gaps due to missing data and cloud cover. The meteorological variables have been extracted from the ECMWF database for both surface and different pressure levels in the atmosphere, which makes this database highly suitable for scaling between low and high spatial resolutions by employing similarity principles (Su, 2002).

2.2. Cloud products

Clouds and precipitation play an essential role in the energy budget and hydrological cycle of the Earth. Clouds reflect shortwave radiation and trap longwave radiation, and thus modulate surface incoming fluxes at short- and long wavelengths. Moreover, clouds are the visible expression of atmospheric condensation processes, and are the prerequisite for precipitation, which is essential for many processes on land. Quantitative estimates of cloud and precipitation properties at high spatial and temporal resolution are of increasing importance for water resource management and for improving our understanding of precipitation processes in climate and weather forecasting models. Although operational networks of weather radars are expanding over Europe and North America, large areas without adequate precipitation information remain. Precipitation estimates from passive satellite imagers may bridge this gap. Polar orbiting satellites can provide information on seasonal and inter-annual variations of cloud and precipitation properties at the global scale, while geostationary satellites can provide information on diurnal variations at quasi-global scales. Considerable focus has also been put to the assessment of various cloud property retrieval algorithms (see for example Stubenrauch et al., 2008 and Stubenrauch et al., 1999).

Several algorithms have been developed to produce surface solar radiation datasets based on radiative transfer calculations and satellite observations (e.g. Bishop and Rossow, 1991; Pinker and Laszlo, 1992; Deneke et al., 2008; Müller et al., 2009). Pinker and Laszlo (1992) use a radiative transfer model to relate the broadband reflectance at the top of the atmosphere to the broadband transmission at the surface, taking account of radiation reductions due to ozone and water vapour, aerosols and clouds. The method proposed by Müller et al. (2009), which is used in the Satellite Application Facility on Climate Monitoring (CM SAF) of EUMETSAT, uses satellite-derived variables to retrieve surface solar irradiance. Their clear-sky irradiance calculations take care of variations in atmospheric water vapour and aerosols, whereas observations from Geostationary Earth Radiation Budget (GERB) instrument are used for the cloudy sky calculations. Alternatively, Deneke et al. (2008) use cloud optical thickness, particle size and cloud phase retrievals to calculate cloudy sky irradiances, whereas the clear sky calculations are climatologically corrected for variations in water vapour and aerosols.

Over the past decades several methods have been developed to detect precipitating clouds and retrieve rain rates. The methods developed for geostationary satellites often use thermal infrared observations, and relate daily minimum cloud top temperatures (Adler and Negri, 1988) or Cold Cloud Durations (CCD) to rain rates (Todd et al., 1995). These methods give fair retrieval accuracies for convective precipitation, but are not suitable for stratiform precipitation. Precipitation retrievals for both stratiform and convective clouds are feasible with the more physically-based microwave radiometer (MWR) based methods (e.g. Wentz and Spencer, 1998). The main drawback of MWR based methods is that they only apply to liquid precipitation and that MWRs are only operated on polar orbiting satellites. Similarly, methods have been developed to derive precipitation from cloud physical properties retrievals of passive imagers (Rosenfeld and Gutman, 1994; Lensky and Rosenfeld, 2006; Roebeling and Holleman, 2009). Because several passive imagers are operated onboard geostationary satellites the retrievals of these methods can be made available at high temporal resolution. However, the use of visible and near-infrared radiances limits the application of these methods to daylight periods only. Beside single instrument retrievals, methods have been developed that combine measurement from different sources. The Climate Prediction Centre MORPHing (CMORPH) method provides global precipitation estimates by propagating motion vectors derived from geostationary satellite infrared observations on passive microwave satellite scans (Joyce et al., 2004). While the Global Precipitation Climatology Project (GPCP) merges measurements from three different sources i.e., precipitation estimates from

low-orbit satellite microwave data, geosynchronous-orbit satellite infrared data, and surface precipitation gauge observations from the Global Precipitation Climatology Centre (GPCC) (Adler et al., 2003).

The cloud properties are important to derive the Surface Solar Irradiance (SSI), and precipitation occurrence and intensity (PRP). The SSI is the incoming solar radiation reaching at the surface, which is mainly determined by the cloud fraction, the cloud optical thickness, and the amount of water vapour and aerosols in the atmosphere. It is of importance to the evapotranspiration theme, since the amount of SSI dominates the amount of energy available for evaporation from the surface and transpiration from the canopies. The precipitation *occurrence* is determined from Cloud Water Path (CWP), effective radius, and cloud phase information, whereas the precipitation *intensity* is calculated from CWP and the thickness of the raining column, which in turn is estimated from the difference between the surface temperature and the cloud-top. Observations from the Spinning Enhanced Visible and InfraRed Imager (SEVIRI) onboard MSG, combined with water vapour profiles from the MEdium Resolution Imaging Spectrometer (MERIS) onboard ENVISAT are used to obtain these cloud properties at regional scale and at high temporal resolution, i.e., Level 2 products that are generated every hour or even every 15 min in case of SEVIRI. The latter temporal resolution is required for regional water and energy balance studies. Observations from the SCanning Imaging Absorption spectroMeter for Atmospheric CartograpHY (SCIAMACHY) onboard the polar orbiting satellite ENVISAT are used to derive SSI at global scale. Time series of SCIAMACHY observations, complemented with observations from its predecessor GOME and GOME-2, provide a solid basis for the generation of Thematic Climate Data Records of SSI, and thus contribute to the comprehensive system of Atmospheric ECVs endorsed by GCOS (GCOS, 2010).

2.3. Water vapour

Water vapour is a key variable in the Earth's water and energy cycle. In the lower troposphere, water vapour is the main resource for clouds and precipitation and the related latent heating dominates the structure of tropospheric diabatic heating (Trenberth and Stepaniak, 2003). In addition, water vapour varies strongly in space and time, acting as the most effective greenhouse gas, and climate models indicate a strong positive radiative feedback (Held and Soden, 2000). Satellite observations provide near-global coverage and thus represent an important source of information, especially over the oceans where radiosonde observations are scarce, and in the upper troposphere where radiosonde sensors are often unreliable. There are about 50 satellite missions that are capable to retrieve atmospheric profiles of humidity or the total column amount (Hollweg, 2005). Various spectral ranges (microwave, infrared, visible, ultraviolet), observation geometries (nadir, limb, and occultation) and retrieval techniques are utilised, each having their own advantages and disadvantages. In addition, satellite observations are used within assimilation methods to generate model-based reanalysis products like ECMWF's ERA-40 (Uppala et al., 2005) and ERA-interim, the Japanese 25-year ReAnalysis (Onogi et al., 2007) and the Modern-Era Retrospective analysis for Research and Applications (MERRA) produced by NASA's Global Modeling and Assimilation Office (GMAO) (Rienecker et al., 2011). Exemplary sensors are the Special Sensor Microwave/Imager (SSM/I) carried aboard Defense Meteorological Satellite Program (DMSP) satellites, the Meteorological Operational satellite (MetOp) Infrared Atmospheric Sounding Interferometer (IASI), the METEOSAT Second Generation (MSG) Spinning Enhanced Visible and Infrared Imager (SEVIRI), the Environmental Satellite (ENVISAT) Medium Resolution Imaging Spectrometer (MERIS) and the MetOp Global Navigation Satellite System Receiver for Atmospheric Sounding (GRAS). Global single and combined sensor products are publicly available: The daily and monthly mean total column water vapour over ice free ocean with a spatial resolution of 0.5° from SSM/I data (Anderson et al., 2010) is available for the time period July 1987 to August 2006 from the Satellite Application Facility on Climate Monitoring (CM SAF) and from the University of Hamburg/Max-Planck-Institute for Meteorology. A similar data set is available from Remote Sensing Systems (Wentz, 1997). Atmospheric water vapour profiles (daily, 5-day and monthly means) gridded on a $1^\circ \times 1^\circ$ latitude-longitude grid for the time period 1985–1999 are part of the TIROS (Television Infrared Observation Satellite) Operational Vertical Sounder (TOVS) Pathfinder Path A dataset (Susskind et al., 1997). Within the GEWEX (Global Energy and Water Cycle Experiment) Global Water Vapour Project (GVaP), the NVAP total column water vapour product was derived from a combination of SSM/I, TOVS and radiosonde data covering the time period 1988–2001 (Randal et al., 1996). Total column water vapour and integrated water vapour for five thick layers based on the Advanced TIROS Operational Vertical Sounder (ATOVS) suite of instruments is provided by CM SAF (Schulz et al., 2009). Available are global daily and monthly means at a horizontal resolution of 90 km × 90 km for the time period from 2004 onwards. Up to now, the ATOVS water vapour products are the only ones for which a merging of different instruments in horizontal space is done over a long time period. Lindenbergh et al. (2008) present a Kriging method for combining Global Positioning System (GPS) and MERIS total column water vapour estimates in space and time for a single day in August 2003.

WACMOS aims at exploring methodologies to deliver enhanced EO water vapour products that exploit the synergies among different observation systems. Two combined products from three different sensors, namely MSG/SEVIRI, ENVISAT/MERIS and MetOp/IASI are developed. The first product combines the high vertical sampling and expected high quality of IASI measurements with the high temporal sampling of SEVIRI data to provide a combined product covering the complete African continent and Central Europe. The second product is based on SEVIRI measurements and MERIS data featuring a high spatial resolution. This product is provided over land only because the MERIS instrument is not capable to observe total column water vapour over oceans with high accuracy and precision. Based on the requirements for water vapour profiles for global numerical weather prediction and climate modelling given by World Meteorological Organization (WMO) (WMO/ReqObs (2001) and WMO/GCOS (2006)) and taking into account the instrument designs, the following technical specification was defined for the proposed WACMOS water vapour products: The combined SEVIRI + IASI water vapour product contains tropospheric water vapour within three vertical layers (200–500 hPa, 500–850 hPa, 850 hPa – surface) at the full MSG disc with a horizontal resolution of 0.25° and is generated for the period from June to December 2008. The SEVIRI + MERIS product contains the total column water vapour for the Elbe/Oder basin on a 0.025° grid for the time period between June and November 2008. A three-hourly temporal resolution (00-03 UTC, 03-06 UTC, etc.) is foreseen for both products. In order to be valuable for use in global numerical weather prediction and climate monitoring, uncertainty requirements are defined for both products. The accuracy (precision) for the combined SEVIRI + IASI product is expected to be better than 0.2 (0.8), 0.6 (2.0) and 0.8 (3.0) kg m^{-2} for the top, middle and bottom layer, respectively. Total column water vapour accuracy and precision for the SEVIRI + MERIS product are expected to be at least 1 kg m^{-2} and 4 kg m^{-2}. Provided the successful development and validation, the expected improvements of the WACMOS water vapour products compared to existing datasets are the combination of benefits from two different sensors and the availability of

the water vapour files plus corresponding error maps. In this case, both products could be generated for a longer time period. Furthermore, the continuation of measurements with similar, future sensors is very likely. On the other hand, it has to be mentioned that both WACMOS products are generated under clear-sky conditions only, because at infrared and near-infrared wavelengths clouds are opaque and do not allow water vapour retrieval. Hence, the clear-sky bias (Lanzante and Gahrs, 2000; Sohn and Bennartz, 2008) compared to all-sky products has to be taken into account when a comparison is done.

3. Methodology and materials

3.1. Evapotranspiration

Evapotranspiration cannot be measured directly from space. Therefore most current algorithms calculate it through the energy balance equation using remotely sensed surface temperature (Kustas and Norman, 2000; Su, 2002; Anderson et al., 2008; van der Tol et al., 2009a). During the last 50 years, a wide range of methods have been developed and evaluated (see reviews by e.g. Glenn et al., 2007; Kalma et al., 2008). The difference between the different methods is the way in which the sensible heat term in the energy balance equation is calculated.

The Surface Energy Balance System (SEBS) model (Su, 2002) is a single source algorithm that calculates the sensible heat through the same physical representation of the turbulent heat exchange for different surface types. In order to include evaporation from water bodies next to the evapotranspiration from land surfaces extra parameterization has been added to the SEBS algorithm in this research. The SEBS algorithm incorporates explicitly the formulation of the roughness height for heat transfer, instead of using fixed values (Su et al., 2001). Since the roughness height for heat transfer can vary with geometrical and environmental variables by several orders of magnitude for different surface types, ignoring the spatial variability of roughness height has led to great uncertainties in estimation of heat fluxes or evaporation using radiometric temperature measurements in several algorithms (e.g. Kalma et al., 2008). Although it is possible to calibrate these algorithms such that their estimates reproduce observations at local scale, it would be very difficult to extend them to regional, continental and global studies by means of satellite observations. These shortcomings are avoided in SEBS.

The turbulent character of the sensible heat is represented by the use of the similarity theories (Kolmogorov, 1991). SEBS iterates over a set of similarity equations using the Monin-Obukhov Similarity Theory (Monin and Obukhov, 1954) for the atmospheric surface boundary layer and the Bulk Atmospheric Similarity Theory (Brutsaert, 1999) for the planetary atmospheric boundary layer that characterize the turbulent exchange of momentum, heat and water vapour. In SEBS, the sensible heat is further constrained by relative evaporative fraction, which is determined by comparing the actual sensible heat flux to that for theoretical wet and dry conditions in order to characterize surface water stress. SEBS is therefore capable of estimating evapotranspiration without the need for local calibration or large numbers of input variables. Three sets of input variables are needed in SEBS. The first set consists of remotely sensed surface variables, including surface albedo, fractional vegetation coverage, emissivity and surface temperature. The second set includes meteorological observations, such as air temperature, vapour pressure and air pressure, and wind speed. The third set of data includes remotely sensed variables of incoming long and shortwave radiation. In WACMOS these variables are obtained through AATSR, MERIS, MODIS sensors and ECMWF model outputs.

3.2. Cloud products

The retrieval of Solar Surface Irradiance (SSI), precipitation occurrence, and precipitation intensity (PRP) from SEVIRI is physically based. It relies on information of the cloud optical properties (cloud optical thickness) and cloud physical properties (cloud condensed water path, cloud phase, and cloud particle effective radius) derived with the Cloud Physical Properties (CPP) algorithm (Roebeling et al., 2006) of the SAF on Climate Monitoring (CM-SAF, Schulz et al., 2009) and water vapour profiles from the MEdium Resolution Imaging Spectrometer (MERIS) onboard ENVISAT. The CPP algorithm retrieves cloud optical thickness, cloud particle effective radius, and cloud thermodynamic phase from observed cloud reflectances at visible (0.6 μm) and near infrared (1.6 μm) wavelengths, following the method described by Nakajima and King (1990). The cloud-top temperature is retrieved from visible (0.6 μm) reflectances and infrared (10.8 μm) cloud radiances (Minnis et al., 1988). The condensed water path is computed from the retrieved cloud optical thickness and cloud particle effective radius. The retrieval of cloud optical thickness, particle size, and cloud phase is done iteratively by matching satellite observed reflectances to look-up tables (LUTs) of simulated reflectances of horizontally and vertically homogeneous water and ice clouds, generated with the Doubling Adding KNMI (DAK) radiative transfer model (Stammes, 2001). The phase "ice" is assigned to pixels for which the observed visible and near-infrared reflectances correspond to simulated reflectances of ice clouds and the cloud top temperature lower than 265 K. The remaining cloud-flagged pixels are considered to represent water clouds. Note that the cloud properties retrievals rely on visible and near-infrared observations, and thus are limited to satellite and solar viewing zenith angles smaller than 72°.

The retrieval of SSI from SEVIRI and MERIS observations is based on the algorithm described by Deneke et al. (2008). This algorithm takes into account variability induced by cloud optical thickness, cloud phase, and particle size from SEVIRI, surface albedo from MODIS, and total precipitable water from MERIS, while for other sources of variability climatological means are used. In its current version, the changes in aerosol properties are neglected. Obviously, this is the largest source of error, in particular for clear sky conditions, while neglecting these properties for cloudy conditions has minor consequences. Radiative transfer simulations are done offline with the DIScrete Ordinate method for Radiative Transfer in vertically inhomogeneous layered media (DISORT) (Stamnes et al., 1988).

The retrieval of global SSI from SCIAMACHY is based on the MAGIC algorithm of Müller et al. (2009) and the FRESCO+ (Fast Retrieval Scheme for Clouds from the Oxygen A-band) algorithm of Wang et al. (2008). The MAGIC algorithm has a look-up-table for the retrieval of clear-sky SSI, taking into account the variability in aerosol properties, water vapour column, surface albedo, and solar zenith angles. For the cloudy pixels (including fully or partly cloudy pixels) MAGIC needs information on the cloud index, which is retrieved from SCIAMACHY observations with the FRESCO+ algorithm. Although SCIAMACHY observes at a low spatial resolution (30 km × 60 km), its high spectral resolution at ultraviolet, visible, and near-infrared wavelengths enables a novel type of cloud observation. The FRESCO+ algorithm retrieves the effective cloud fraction, which is directly related to the cloud index of the MAGIC algorithm, and cloud pressure from the TOA reflectance at three wavelengths (758, 760, and 765 nm). Due to the presence of clouds, the reflectance at 758 nm is larger than for a clear-sky scene, whereas the depth of the strongest O_2 absorption band at 760 nm and of the weaker O_2 absorption band at 765 nm varies according to the height and the optical thickness of the cloud. The FRESCO+ algorithm fits a simulated reflectance spectrum to the measured

reflectance spectrum for the three wavelengths to retrieve the effective cloud fraction and cloud pressure. The SCIAMACHY SSI product is generated from the FRESCO orbit data (Level 2) and is regridded to monthly mean global maps. The retrieval of precipitation occurrence and intensity is based on the approach presented by Roebeling and Holleman (2009). Their approach uses information on condensed water path, particle effective radius, and cloud thermodynamic phase to detect precipitating clouds, while information on condensed water path and cloud top height is used to estimate rain rates. A simple but adequate model proposed by Petty (2001) is used to calculate evaporation of rainfall below cloud base. This procedure uses monthly mean water vapour retrievals from MERIS, cloud top height, and cloud optical thickness retrievals from SEVIRI to estimate cloud base height. The fact that the approach of Roebeling and Holleman (2009) can be applied to geostationary observations from SEVIRI potentially allows for the provision of precipitation observations over the entire MSG disk, covering Europe and Africa every 15 minutes.

3.3. Water vapour

Input variables to the water vapour products are SEVIRI Level 1.5 data that are navigated and calibrated brightness temperatures, MERIS reduced resolution total column water vapour with a spatial resolution of 1.2 km and the water vapour profiles (43 vertical levels) obtained from IASI. The retrieval of the MERIS water vapour content has been performed using the algorithms described in Fischer and Bennartz (1997) as well as Bennartz and Fischer (2001). The MERIS data is processed and provided by ESA. The IASI level 2 product is processed at Deutscher Wetterdienst using the algorithm of Schwärz (2004). SEVIRI Level 2 water vapour profiles (43 levels) are obtained employing a physical retrieval scheme (EUMETSAT, 2010) developed within the EUMETSAT Satellite Application Facility (SAF) on Support to Nowcasting and Very Short-Range Forecasting (NWC SAF). Since the retrieval is done for clear sky pixels only, the SEVIRI cloud mask, part of the NWC SAF MSG software package and available from CM SAF, is a mandatory retrieval input. The cloud mask algorithm is described in Derrien and LeGléau (2005). The SEVIRI total column water vapour (TCWV) as well as the layered column water vapour (LCWV) for SEVIRI and IASI are determined by vertically integrating the water vapour profiles. Since the IASI and SEVIRI retrieval are based on optimal estimation theory, a measure of uncertainty is obtained as well. In case of MERIS, an uncertainty of 10% relative to the water vapour amount is assumed for land pixels (MERIS PQSR, 2006).

For both WACMOS water vapour products an objective analysis method (Kriging) is applied to interpolate data in space and time with the possibility to also provide uncertainty information for the combined products. Kriging is a geostatistical method which is currently applied in diverse disciplines like e.g. hydrology (Goovaerts, 2000) and meteorology (Lindenbergh et al., 2008). The approach of Lindenbergh et al. (2008), who combined MERIS TCWV observations with hourly ground based Global Positioning System (GPS) observations of a single day, is applied. In case of the SEVIRI + MERIS product, the combined integrated total water vapour column $\hat{x}(p_0, t_S)$ at location p_0 and time t_S (i.e. one grid point and 3-hour interval) is predicted as a linear combination

$$\hat{x}(p_0, t_S) = \sum_{i=1}^{n} \lambda_i (x_S(p_i, t_S) + \Delta x_S(p_i, t_S)) + \nu (x_M(p_0, t_M) + \Delta x_M(p_0, t_M)) \quad (1)$$

of SEVIRI observation $x_S(p_1,t_S)$, $x_S(p_2,t_S)$, …, $x_S(p_n,t_S)$ made at n different grid points at time t_s and one MERIS observation $x_M(p_0,t_M)$ at the same pixel (p_0), obtained at time t_M. Δx_S and Δx_M denote the SEVIRI and MERIS retrieval error, respectively. The challenge is to determine the optimal weights (λ_1, …, λ_n,ν) for each observation. If a time series of M measurements at each location p_i is available, a reasonable requirement is that the mean squared deviation between prediction $\hat{x}(p_0, t_S)$ and truth $x(p_0, t_S)$ is minimal. This leads to a set of $(n+1)$ equations where the single terms are covariances between the different measurements, like e.g. the spatial covariance among the SEVIRI observations, the spatiotemporal covariances between the MERIS observation and the n SEVIRI measurements and the temporal covariance between the existing MERIS observations and the collocated prediction point. If the covariances are known, the weights can be determined and Eq. (1) directly yields the optimal TCWV estimate at the considered grid point.

In case of the SEVIRI + IASI product, the approach is similar, except that the Kriging is performed separately for the three vertical layers in order to obtain a merged water vapour profile.

Before the Kriging is applied, systematic differences between the datasets to be combined are eliminated. Based on the monthly means of the individual data, a bias is determined for each pixel and a bias correction is applied to the 3-hourly measurements. SEVIRI (for SEVIRI + IASI) and MERIS (for SEVIRI + MERIS) are used as the reference, because better quality water vapour information was found from validation investigations.

4. Retrieval results and validations

4.1. Evapotranspiration

Actual latent heat flux cannot be measured directly from remote sensing imagery, but needs to be estimated as the "residual" of the energy balance equation. Thus, besides the validation using ground based measurements, the estimated actual evapotranspiration can be validated by validating the individual components of the energy balance equation: net radiation, sensible heat flux and ground heat flux. In addition, instantaneous values for the surface heat fluxes are scaled up to daily values using the evaporative fraction, thus the upscaling technique needs an evaluation too. The validations of these fluxes are currently hardly possible at global scale, because no observed global products of net radiation, ground heat flux, or sensible heat flux exist for comparison. Instead the validation needs to be performed against field measurements at local scales.

The mostly used ground based measurements are the Bowen ratio method (Pauwels and Samson, 2006), eddy covariance (Baldocchi et al., 2001; Van der Kwast et al., 2009) and scintillometry (Pauwels et al., 2008). In the Bowen ratio method the energy balance is partitioned into one part that is used for sensible heat and another part for latent heat. The ratio of these two is the Bowen ratio, which is controlled by the difference in air temperature and humidity at two heights in the air above the surface. In the eddy covariance method the latent heat flux is estimated directly by measuring the water vapour concentration in upward and downward eddies, simultaneously with their velocity. In scintillometry the sensible heat flux is calculated by measuring the refraction index of the air over a specified distance. The reader is referred to Verhoef and Campbell (2005) for details in evaporation measurement.

The validation is complicated by scale differences between field measurements and the remote sensing imagery. Not only have the field measurements a different footprint (only the scintillometer measurement has a footprint in the order of the pixel size of the WACMOS product), the revisit time of certain satellites also prohibits comparison of long time series. The revisit time of the remote sensing sensors combined with cloud coverage limits the number

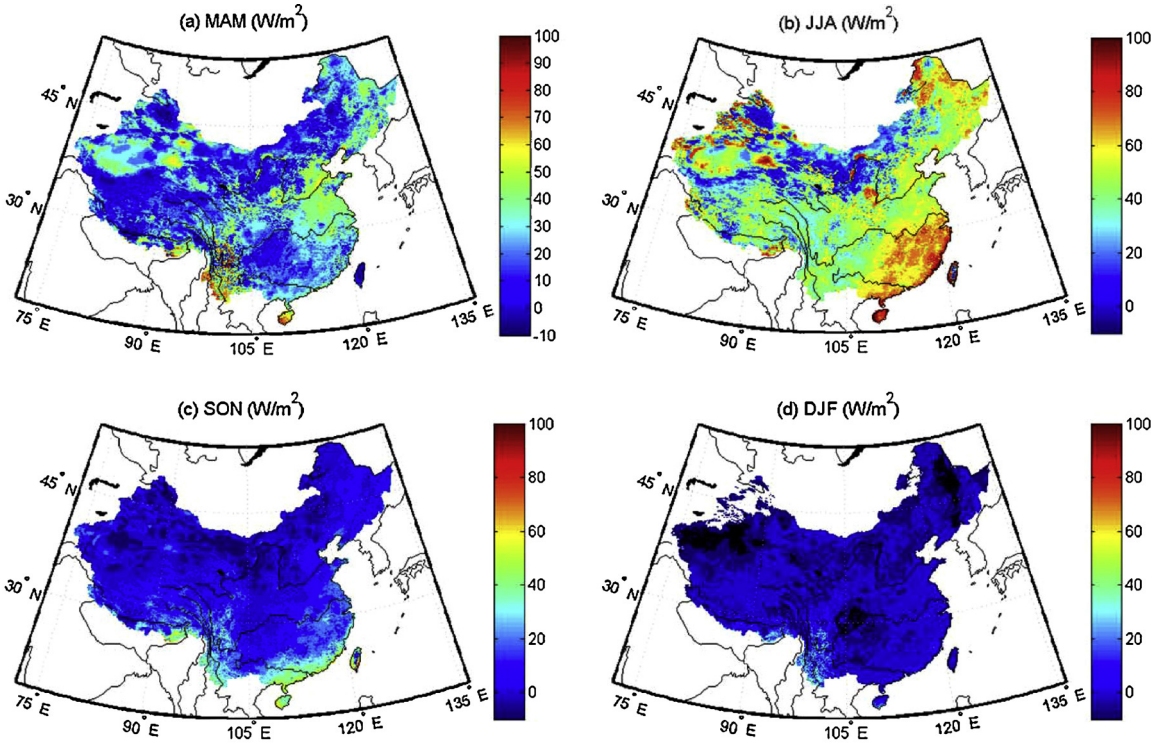

Fig. 1. SEBS derived 10 years monthly 0.1 × 0.1 degree latent heat fluxes 1 es in China.

of remote sensing images that can be used for validation purposes. This problem can be circumvented by using a validated Soil Canopy Observation, Photochemistry and Energy fluxes (SCOPE) model (van der Tol et al., 2009b) to interpolate between satellite overpasses (Timmermans et al., 2013).

The SCOPE model is a soil-vegetation- atmosphere model that couples radiative transfer of optical and thermal radiation with leaf biochemistry processes. It is able to simultaneously estimate from the meteorological forcing the vertical distribution of within-canopy canopy heat fluxes, the aerodynamic resistances (Verhoef et al., 1999) and the hyperspectral outgoing radiances (Verhoef et al., 2007). These radiances can be used as input for a sensor simulator that is attached to the model. The advantage of simulating AATSR radiances is that uncertainties in the atmospheric correction are circumvented and that we have 'measurements' even for cloudy days. The model therefore provides both the variables needed as input for SEBS (meteorological variables, the remote sensing imagery) and the outputs (surface fluxes) such that the parameterizations in SEBS can be evaluated.

An example for the validation is given by Timmermans et al. (2013). The methodology was then applied to validate the individual heat fluxes for other in-situ measurement sites in Europe and afterwards to evaluate the methodology for interpolating actual evapotranspiration to daily values. Through these validations, it was discovered that the original parameterizations caused in general an underestimation of the soil heat flux and sensible heat flux. The underestimation of the soil heat flux originated from the use of the fractional vegetation cover. This parameter tends to saturate very quickly to values for full canopy, although ground measurements showed otherwise. The new parameterization solved this problem by incorporating the leaf area index for separation between bare soil and fully developed vegetation (Timmermans et al., 2013).

The underestimation for sensible heat flux originated because the formulation of the kB^{-1} (Su et al., 2001) did not represent explicitly dense vegetation with high leaf area index values. For canopies with high LAI values, radiation only penetrates the top part of the canopy. This part dominates as source for the sensible heat, and consequently the virtual height of this source should be higher than the original kB^{-1} formulation predicted. These extra formulations for high LAI values improved the correlations from −0.07 to 0.86 for the sensible heat flux for the Sonning site in Reading (Timmermans et al., 2013).

In further validations the new parameterizations for estimating LAI, ground heat flux and the roughness length for heat transfer are used (Timmermans et al., 2013; Chen et al., 2012a). Based on the advancement of knowledge on turbulent flux parameterization method, the method for estimating the roughness length of heat transfer has been updated with diurnal pattern information included (Chen et al., 2012a). The performance of new revisions of SEBS was evaluated by time series observations at different land cover and climatelorlogical environment (Chen et al., 2012a). High resolution satellite products generated with the new SEBS parameterizations were verified at complex topographical area with better performance than the old version (Chen et al., 2012b). This progress makes SEBS ready for generating global evapotranspiration product at 10–100 m spatial resolution when the computing resource becomes sufficient in future.

SEBS was then used to derive a 10 years monthly 0.1 × 0.1 degree latent heat flux with currently available EO variables in China. The four seasonal spatial patterns are shown in Fig. 1. The Southeast of Tibetan Plateau, Yunnan and south part of Sichuan province have the highest latent heat flux. Gobi desert in Northwest of China has the lowest annual latent heat flux, followed by the Western Tibetan Plateau and Inner Mongolia. The Yangtze and Yellow river regions have relative high latent heat fluxes. The observational dataset includes Qomolangma station (QM), Nam Co Station, Linzhi Station of Chinese Academy of Sciences (Ma et al., 2008), Maqu (MQ)(Chen et al., 2012b; Wang et al., 2013), Wenjiang (WJ) (Zhang et al., 2012), Bijie (BJ) (Ma et al., 2006), Miyun (MY) (Jia et al., 2012), Daxing (DX) (Liu et al., 2001), Guantao (GT) (Jia et al., 2012; Liu et al., 2001), Yucheng (YC) (Flerchinger et al., 2009). The correlation coefficient

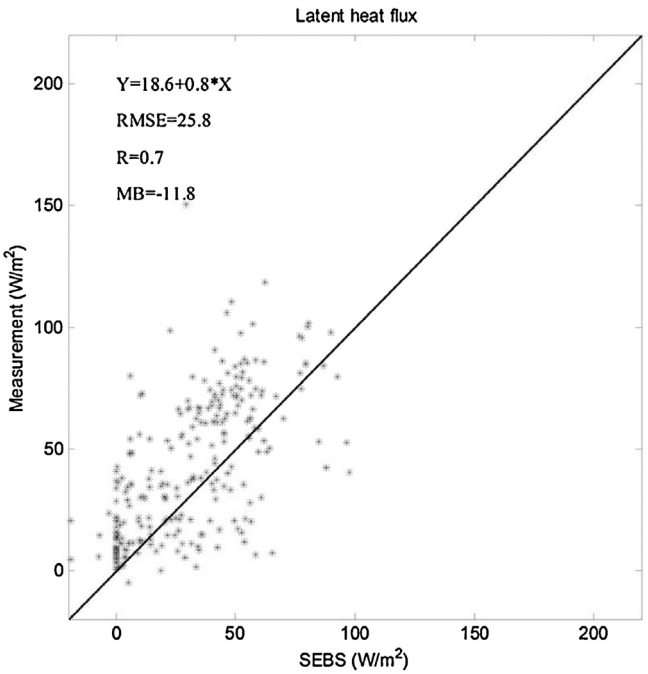

Fig. 2. Validation of SEBS derived latent heat fluxes with observational datasets from Qomolangma station (QM), Nam Co Station, Linzhi Station of Chinese Academy of Sciences (Ma et al., 2008), Maqu (MQ) (Chen et al., 2012b; Wang et al., 2013), Wenjiang (WJ) (Zhang et al., 2012), Bijie (BJ) (Ma et al., 2006), Miyun (MY) (Jia et al., 2012), Daxing (DX) (Liu et al., 2011), Guantao (GT)(Jia et al., 2012; Liu et al., 2011), Yucheng (YC)(Flerchinger et al., 2009).

between SEBS estimates and observations is 0.7 with $-11.8\,W\,m^{-2}$ MB (mean bias) and $25.8\,W\,m^{-2}$ RMSE (Fig. 2).

In SEBS the actual daily evapotranspiration is extrapolated using the evaporative fraction which is considered constant during the day. However, in wintertime the evaporative fraction has not reached its equilibrium state at the time of the satellite overpass, which can cause an overestimation of the daily evapotranspiration during this season. The solution for this problem is to use geostationary satellite imagery to estimate the diurnal pattern of evaporative fraction and correct for this effect. As merging of orbiting and geostationary satellite products is computationally challenging for the large data volume involved, the current WACMOS product focuses first on the creation of a global evapotranspiration product using only orbiting data.

4.2. Cloud products

An example of the SSI product retrieved from SEVIRI and MERIS observations is presented in Fig. 3. Note that the gap in the centre of the image corresponds to sun glint viewing geometries for which the SSI retrievals are omitted. Fig. 4 shows an example of the global monthly mean SSI for July 2008 as retrieved from SCIAMACHY. The latitudinal gradient of surface solar irradiance is clearly observed from the monthly mean map. The ITCZ and stratocumulus cloud fields west of the continents show low SSI, while high SSI occurs over the Sahara desert.

The SCIAMACHY Solar Surface Irradiance retrievals were compared against ISCCP-Flux Dataset (FD) Shortwave Downwelling Fluxes (SDF). The difference between monthly mean SCIAMACHY SSI and ISCCP was within $-12\,W\,m^{-2}$, with a standard deviation of $62\,W\,m^{-2}$ (Wang et al., 2011). The validity of the SSI products from SCIAMACHY and SEVIRI is determined through a comparison against ground-based measurements of the Baseline Surface Radiation Network (BSRN). The SCIAMACHY product was validated for

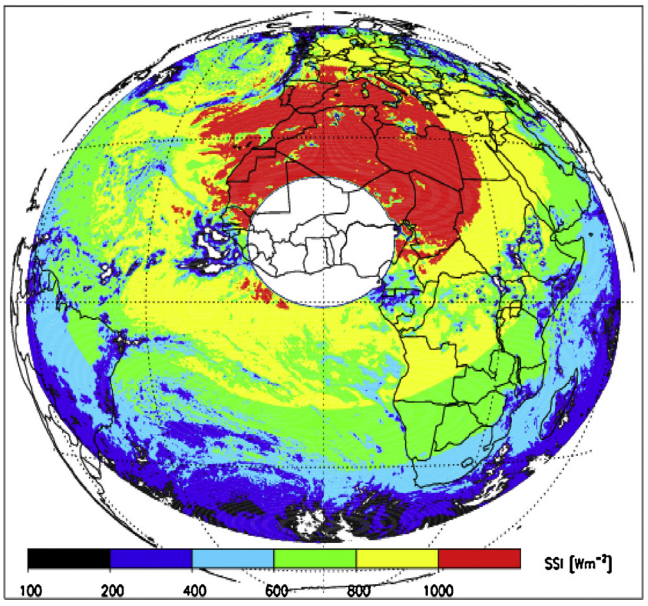

Fig. 3. An example of instantaneous MSG-SEVIRI SSI products for 1 July 2008 at 12:00 UTC.

one year against 19 BSRNs stations, while the SEVIRI product was validated for 5 months against 6 BSRN stations.

Fig. 5 presents the validation results for three BSRN stations in Europe, which show that instantaneous SSI retrievals from SCIAMACHY and daily averaged SEVIRI retrievals agree well with the respective ground-based irradiance values. The precision (RMSE) is about $75\,W\,m^{-2}$ for SCIAMACHY and about $25\,W\,m^{-2}$ for SEVIRI. The accuracy (bias) for SEVIRI and SCIAMACHY is about $3\,W\,m^{-2}$ and $10\,W\,m^{-2}$, respectively. The evaluation results are in line with findings of Deneke et al. (2008), who validated an earlier version of the SSI algorithm with one year of pyranometer measurements from 35 stations over the Netherlands. Because the Cabauw station is located in a flat and homogenous grassland terrain at sea level, the BSRN measurements taken at this station are more likely to represent the area of a satellite pixel. At BSRN stations that are located in more heterogeneous terrain, larger variations between satellite-retrieved and BSRN-observed SSI values are expected. These larger variations are due to among others the height above sea level, horizontal view restrictions, multiple reflection effects, or shadow effects. Especially the SCIAMACHY retrievals, which represent an area of $30\,km \times 60\,km$ at nadir, are subject to lower precision over

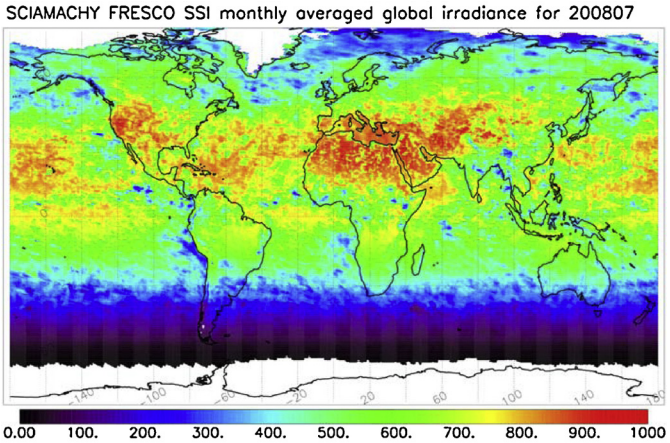

Fig. 4. An example of the global means SSI in $W\,m^{-2}$ from SCIAMACHY for July 2008.

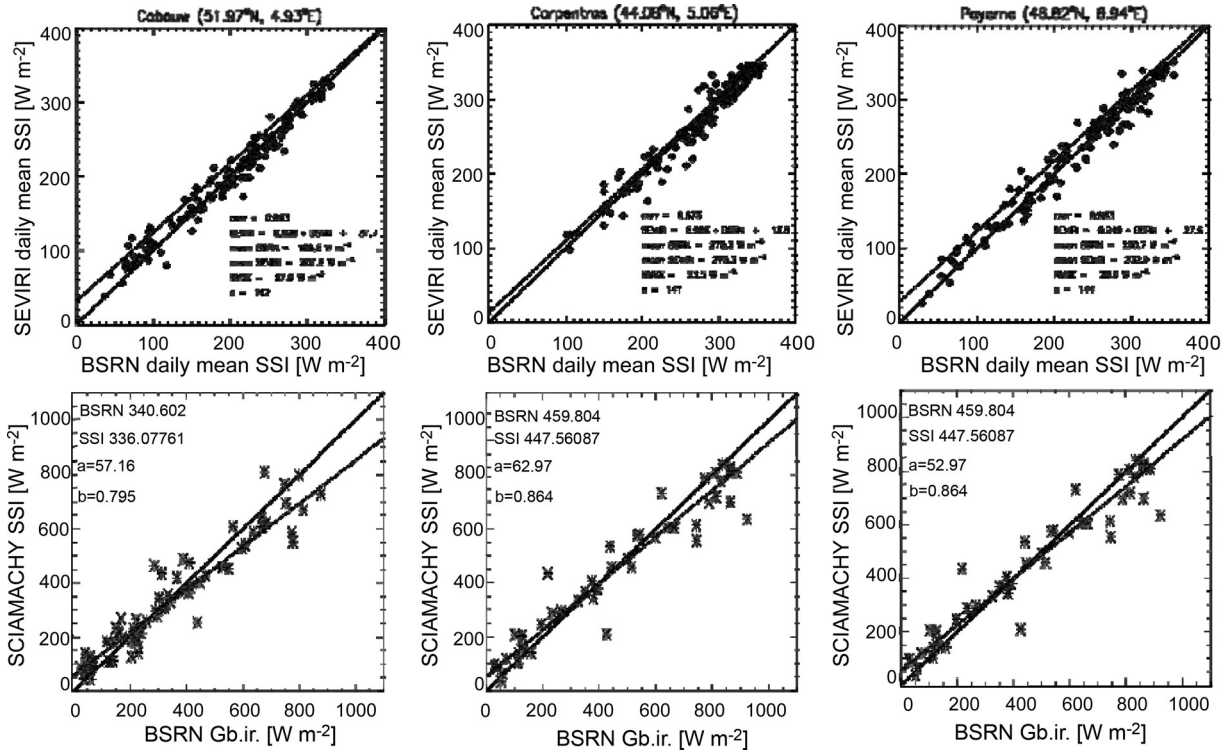

Fig. 5. Comparison of solar surface irradiance (SSI) retrieved from SEVIRI cloud physical properties (top panels) and from SCIAMACHY effective cloud fraction (bottom panel) against BSRN observations taken at Cabauw (the Netherlands), Carpentras (France), and Payerne (Switzerland). The SEVIRI values are represented as daily means for May – September 2008, while the SCIAMACHY values represent instantaneous observations taken approximately once every six days at about 10:00 LT for the year 2008. Solid lines denote the 1:1 relation, while dashed lines denote linear fit results.

heterogeneous terrains. The SSI retrievals from SEVIRI, which have a spatial resolution of 3 km × 3 km at nadir, will be more precise over heterogeneous terrain. The latter precision may further improve when KNMI introduces an improved SSI product for SEVIRI that also uses information from the high-resolution visible (HRV) channel (Deneke and Roebeling, 2010).

Examples of monthly mean precipitation occurrence and intensity are presented in Fig. 6.

The precipitation occurrence and intensity products from SEVIRI are validated against two types of reference instruments, i.e., the Tropical Rainfall Measuring Mission Precipitation Radar (TRMM-PR) and ground-based weather radar observations. The validity of these products was demonstrated over Western Europe (50°–55°N, 3°–8°E) by Roebeling and Holleman (2009) and over West Africa (0°–20°N, 10°W–10°E) by Wolters et al. (2011). Although both studies validate the SEVIRI precipitation products over different climate regions and with different reference instruments, similar validation results are found. Fig. 7 present the relationship between SEVIRI-retrieved and reference instrument-observed areal mean precipitation occurrence and rain rate. It can be seen that the areal mean precipitation occurrences from SEVIRI and the reference instruments are highly correlated (corr. ≈ 0.9), while the areal mean rain rate retrievals are weaker correlated (corr. ≈ 0.6). At pixel level, the SEVIRI retrievals have an acceptable accuracy (bias) of about 0.1 mm h^{-1} and a precision (standard error) of about 0.8 mm h^{-1} (Roebeling and Holleman, 2009). Mismatches between the re-projected SEVIRI and reference instrument images, due to differences in observation time, parallax shift, and collocation errors hinder the comparison of both images. Here the parallax shift is the apparent displacement of an observed cloud, which occurs because SEVIRI observes the Earth under an oblique angle.

4.3. Water vapour

In the following, representative results are shown and discussed. A more thorough analysis dealing with the WACMOS water vapour products only will be published in a separate paper.

An example for the merged SEVIRI + IASI water vapour product at the time interval 12–15 UTC on August 5th 2008 is presented in Fig. 8. For each plot a corresponding error map exists but is not shown here. The main information certainly comes from the SEVIRI instrument which provides measurements of the full disk at every time step. Nevertheless, the available IASI information between 12–15 UTC results in a finer structure over the region covering the Atlantic Ocean between Iceland and South America and parts of Brazil.

The merged total column water vapour (TCWV) from SEVIRI and MERIS over the Elbe/Oder basin at 12-15 UTC on August 5th 2008 and the corresponding error map are shown in Fig. 9. The TCWV reaches values up to 30 kg m^{-2}. The error is below 1.5 kg m^{-2} for most pixels and gets up to 4 kg m^{-2} in some cases. The information for the merged product comes from the SEVIRI observations between 12 and 15 UTC and the MERIS measurements from the overpass around 10:15 UTC, i.e. the previous three-hour interval. Compared to the TCWV obtained from SEVIRI only (not shown), the combined product shows a finer spatial structure originating from the MERIS information.

The validation of the WACMOS water vapour products is mainly based on comparisons to radiosonde measurements at Global Climate Observing System (GCOS) Upper Air Network (GUAN) stations. Ground-based remote sensing observations from the Meteorological Observatory Lindenberg (MOL), Germany, are utilised, too. In addition, the water vapour products are also compared to other satellite based water vapour retrievals, e.g.,

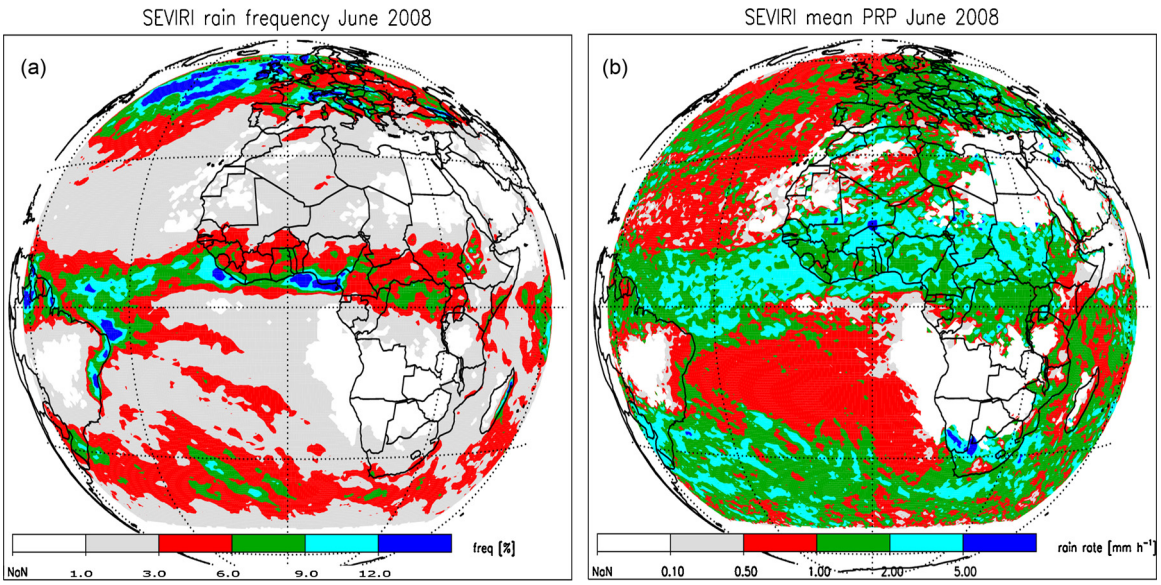

Fig. 6. Examples of monthly mean precipitation occurrence (A) and intensity (B) product for July 2008. Note that these products were calculated from daytime observations between 6 and 18 h.

from Moderate Resolution Imaging Spectroradiometer (MODIS), Advanced TIROS Operational Vertical Sounder (ATOVS), and Special Sensor Microwave Imager (SSM/I). Here, the focus is on two approaches: The validation of the SEVIRI + IASI product with radiosonde measurements and the comparison of the merged TCWV from SEVIRI + MERIS with MODIS data. In both cases results for August 2008 are presented.

Temporally and spatially collocated and quality checked radiosonde observations form the basis of the SEVIRI + IASI product validation. The difference between the WACMOS and the radiosonde water vapour products are computed and systematic differences (biases) and bias corrected RMS error are determined at monthly basis as averages over all temporal and spatial entries. For August 2008 the obtained results are presented in Table 3. The

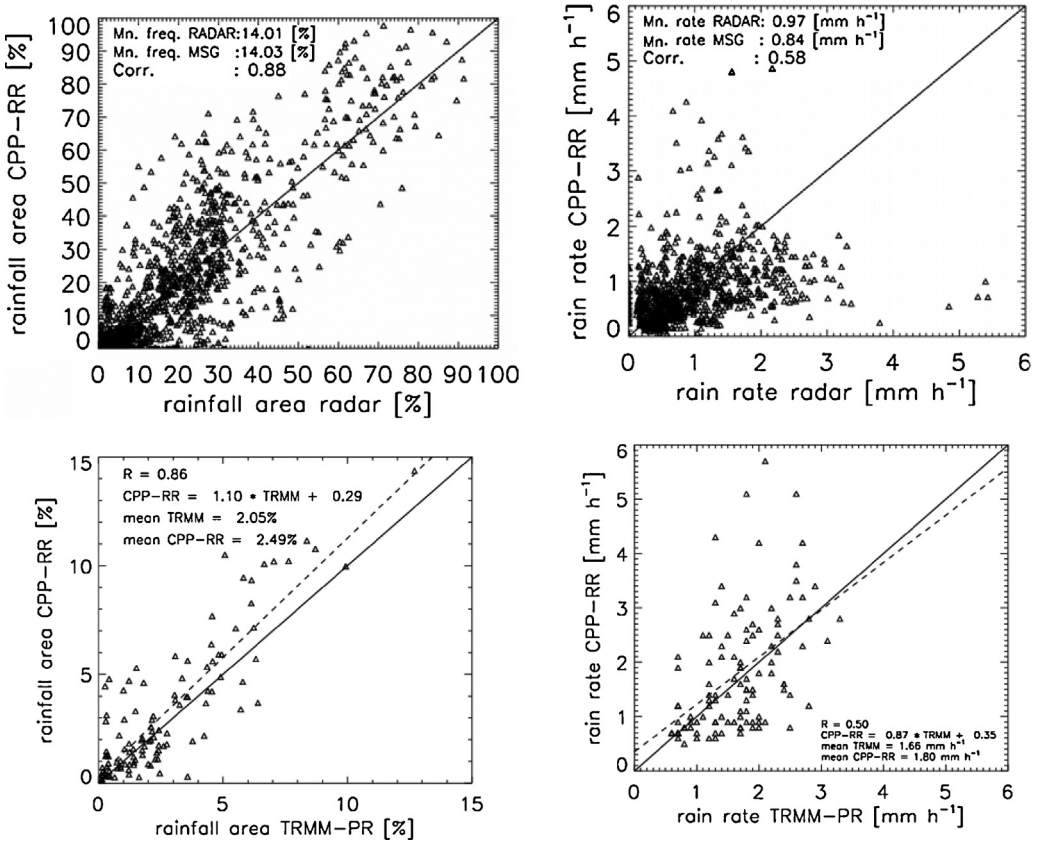

Fig. 7. Scatter plots of SEVIRI retrieved versus reference instrument observed areal mean precipitation occurrences (left panels) and rain rates (right panels). 1 The upper panel shows the plots of CPP-RR versus weather radar for central Europe. The lower panel shows the plots of CPP-RR versus TRMM-PR for Western Africa.

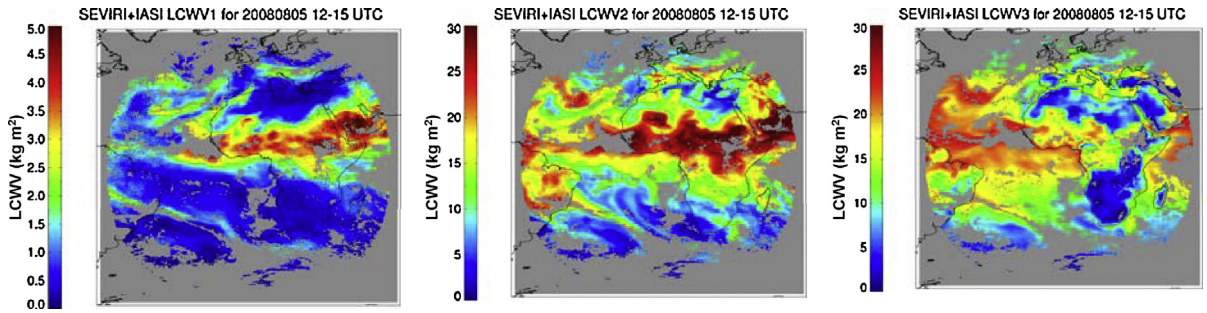

Fig. 8. Layered column SEVIRI+IASI water vapour for the time interval 12-15 UTC on August 5th 2008. Left: Layer 1 between 200 and 500 hPa. Middle: Layer 2 between 500 and 850 hPa. Right: Layer 3 between 850 hPa and surface. Cloudy areas and pixels outside the region of interest are in grey.

Table 3
Bias and bias corrected RMS of the layered column water vapour (LCWV) between GUAN radiosond1 es and SEVIRI, IASI and the merged SEVIRI+IASI product for August 2008. The WACMOS water vapour technical specifications (TS) are also given.

Parameter		SEVIRI	IASI	SEVIRI+IASI	WACMOS TS
Bias ($kg\,m^{-2}$)	LCWV1	0.11	0.24	−0.001	0.2
	LCWV2	0.86	0.95	0.83	0.6
	LCWV3	−0.21	−1.43	−0.23	0.8
RMS ($kg\,m^{-2}$)	LCWV1	0.55	0.52	0.58	0.8
	LCWV2	2.91	2.05	3.27	2.0
	LCWV3	2.60	2.85	2.93	3.0

results for the single sensor product, i.e. SEVIRI and IASI as well as the WACMOS technical specifications are given, too. In terms of biases, SEVIRI product performs better than the IASI one for all three vertical layers. This is the reason why SEVIRI was chosen as reference for the bias correction. Currently, an IASI assessment of various IASI retrieval schemes is carried out, also focusing on an analysis of the observed bias. Final results are expected in late 2011. For the merged product, the biases are comparable to the ones obtained for SEVIRI only. The biases for LCWV1 and LCWV3 are within the WACMOS technical specifications. On the other hand, the LCWV2 bias exceeds the value defined in the technical specifications.

To validate the SEVIRI + MERIS product radiosonde data are not appropriate, because only three GUAN stations are located within the product's geographical region. As a consequence the number of collocations is too small to get good statistics. Therefore a comparison with the Moderate Resolution Imaging Spectroradiometer (MODIS) was done. The AQUA MODIS total column water vapour (MYD05, collection 5), obtained from the NASA Level 1 and Atmosphere Archive and Distribution System (LAADS), for August 5th 2008 is shown in Fig. 9. Since AQUA passed Central Europe around 12:50 UTC, the MODIS measurements can be compared to the merged SEVIRI + MERIS product in Fig. 9. Two conclusions can be drawn: (1) some differences in the cloud mask can be observed; (2) higher water vapour amounts are obtained with MODIS. For the selected case, the bias between the SEVIRI + MERIS product and MODIS is $-1.62\,kg\,m^{-2}$, i.e. the bias is outside the accuracy

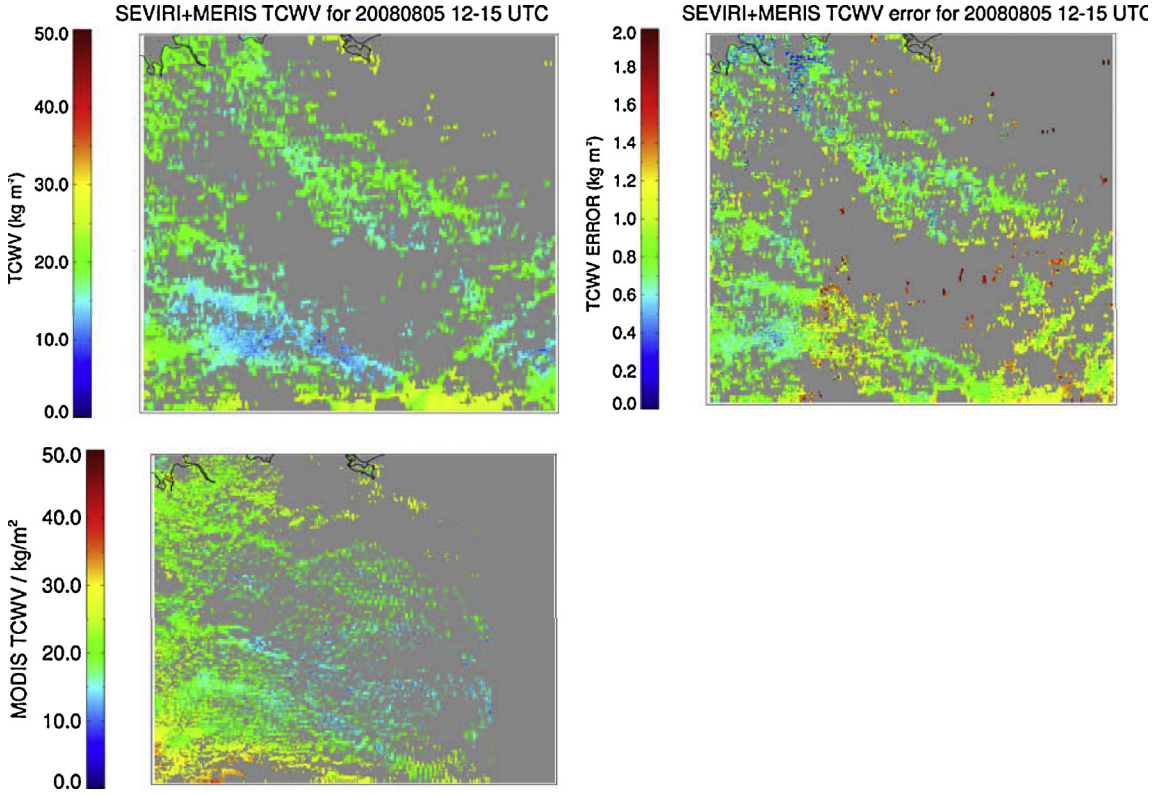

Fig. 9. Total column water vapour (top left) and error (top right) obtained from the Kriging of SEVIRI and MERIS for August 5th 2008 12-15 UTC. The AQUA/MODIS total column water vapour (NASA LAADS MOYD05 product) for 20080805 around 12:50 UTC is also shown (bottom). Cloudy regions are in grey.

of 1 kg m^{-2} aimed for. Performing the same validation for SEVIRI and MERIS separately yields mean biases of −1.03 kg m^{-2} (SEVIRI) and −2.86 kg m^{-2} (MERIS). Hence, the quality of the merged product is between the one of the single sensor data and the negative bias of the merged product is caused by the large bias between MERIS and MODIS. One possible explanation could be an overestimation of the TCWV by MODIS. Li et al. (2003) reported that the MODIS near-infrared total column water vapour column appears to overestimate the TCWV compared to radiosonde measurements. Also, in a comparison of hourly estimates of the total column water vapour over India using different measurement techniques, MODIS is found to be overestimating the TCWV (Prasad and Singh, 2009). Consequently, the bias to MODIS rather originates from the quality of the retrieval schemes than the combination technique. In addition, the currently available MERIS data used here is based an older MERIS algorithm (2nd reprocessing) which is known to result in a lower TCWV content than the updated version (R. Leinweber, FU Berlin, Germany, pers. comm.). It is expected that the upcoming MERIS reprocessing at ESA will increase the quality of the MERIS TCWV product.

Based on the validation shown, it can be concluded that the Kriging seems to work efficiently. The quality of the merged products is within the range spanned by the individual data sets and whenever the WACMOS product is outside the WACMOS technical specification, the single sensor products are also not meeting the required accuracy. Hence, it is currently investigated how the accuracy of the individual products, especially IASI and MERIS could be improved.

5. Conclusions

In order to understand the role of the global water cycle in the Earth system it is essential to be able to measure hydro-climatic variables, such as radiation, precipitation, evapotranspiration, soil moisture, clouds, water vapour, surface water and runoff, vegetation state, albedo and surface temperature, etc. Such measurements are required to further increase not only our understanding of the different components of the water cycle and its variability, both spatially and temporally, but also to characterise the coupling between the terrestrial and atmospheric branches of the water cycle and to quantify how this coupling may influence climate variability and predictability. Moreover, enhancing the observational capacity and the model capabilities to predict in a reliable manner the variations in the global water cycle will be a key contribution to the improvement of water governance, the mitigation of water-related damages and sustainable human development.

In the last few years, earth observation has demonstrated the capacity to provide reliable measurements over oceans, land and atmosphere representing a unique tool for scientists to observe and monitor the earth system. A new era of earth observation has emerged with ever increasing number of missions and sensors available for scientific and operational applications. However, in order to fully exploit this increasing potential and bring this newly available capacity to practical operational levels, significant scientific efforts are required. The Water Cycle Multi-mission Observation Strategy (WACMOS) project is one such effort.

Since the launch of the WACMOS project significant progress has been made in developing and validating a novel set of four thematic algorithms and example geo-information products relevant to the water cycle: evapotranspiration, soil moisture, cloud characterization, and water vapour. The generation of these products is based on a number of innovative techniques and methods using multi-mission based strategies to improve current observations, thus demonstrating the potential of the synergistic use of the different types of information to be provided by current and future observation systems. In the current phase of the project, emphasis has been put on the development of the methodologies and their validation strategies, as well as the generation of the preliminary demonstration data sets. More specific achievements are summarised as follows:

Evapotranspiration: A new parameterization for the ground heat flux is developed for the SEBS algorithm, and a new validation method is proposed using a remote sensing product simulator with the SCOPE model. The system as such is capable to generate turbulent heat fluxes and evapotranspiration using optical and thermal sensors like MERIS and AATSR among others on global scale.

Soil moisture: A merged multi-sensor soil moisture climatology is generated for the period 1978–2008 by merging active and passive microwave soil moisture data records for the first time. The consistency of the merged product is demonstrated using limited in-situ observations (Dorigo et al., 2010).

Cloud products: The cloud properties generated include Solar Surface Irradiance (SSI) and precipitation occurrence and intensity. Observations from the SEVIRI instrument are combined with water vapour profiles from the MERIS instrument to obtain these cloud properties at regional scale and at high temporal resolution at every hour or even every 15 min. Observations from the polar orbiting SCIAMACHY instrument is used to derive SSI at global scale. Due to the calibration units on-board SCIAMACHY, and its predecessors GOME and GOME-2, the SSI retrievals from these instruments have high potentials for the construction of Thematic Climate Data Records with high stability and homogeneity, and complement the SSI datasets that have been assessed within GEWEX.

Water vapour: For the first time SEVIRI and MERIS as well as SEVIRI and IASI observations have been successfully combined into a water vapour product using a geostatistical approach. Systematic deviations between the combined SEVIRI and MERIS product and other (MODIS) satellite products are noticed which are caused by differences in the cloud mask and the individual retrieval schemes rather than the combination methodology.

Despite these preliminary important achievements, it is evident that the production of global water cycle products fulfilling the GCOS ECVs requirements will require substantially bigger efforts. It is strategically important and opportune to continue and intensify the present efforts, such that the developed methodologies and the validation strategies can be further applied to reprocessed satellite data records to generate global water cycle products for the improvement of water governance, the mitigation of water-related damages and sustainable human development. Further information and details of data products can be obtained at the website wacmos.org.

Acknowledgements

The WACMOS project was funded by the STSE programme of the European Space Agency. The WACMOS team is grateful to the members of the Expert User Advisory Committee (Peter Bauer, Ad de Roo, Rick Lawford and Peter van Oevelen) for their scientific supports and advices in the course of the project. K. Hungershöfer, M. Schröder and J. Schulz thank the NWC SAF team, especially Miguel A. Martinez (AEMET) for their support concerning the new SEVIRI Physical Retrieval and R. Lindau from the University of Bonn, Germany, for fruitful discussions on the Kriging.

References

Adler, R.F., Negri, A.J., 1988. A satellite IR technique to estimate tropical convective and stratiform rainfall. J. Appl. Meteorol. 27, 30–51.

Adler, R.F., Huffman, G.J., Chang, A., Ferraro, R., Xie, P., Janowiak, J., Rudolf, Schneider, U., Curtis, S., Bolvin, D., Gruber, A., Susskind, J., Arkin, P., Nelkin, E., 2003. The version 2 Global Precipitation Climatology Project (GPCP) monthly precipitation analysis (1979-Present). J. Hydrometeor. 4, 1147–1167.

Aires, F., Prigent, C., 2006. Toward a new generation of satellite surface products? J. Geophys. Res. 111, D22S10, http://dx.doi.org/10.1029/2006JD007362.

Anderson, A., Fenning, K., Klepp, C., Bakan, S., Graß, H., Schulz, J., 2010. The Hamburg Ocean Atmosphere Parameters and Fluxes from Satellite Data–HOAPS-3. Earth. Syst. Sci. Data 2, 215–234, http://dx.doi.org/10.5194/essd-2-215-2010.

Anderson, M.C., Kustas, W.P., Norman, J.M., 2007. Upscaling flux observations from local to continental scales using thermal remote sensing. Agron. J. 99, 240–254.

Anderson, M.C., Norman, J.M., Kustas, W.P., Houborg, R., Starks, P.J., Agam, N., 2008. A thermal-based remote sensing technique for routine mapping of land-surface carbon, water and energy fluxes from field to regional scales. Remote Sens. Environ. 112, 4227–4241.

Baldocchi, D., Falge, E., Gu, L.H., Olson, R., Hollinger, D., Running, S., Anthoni, P., Bernhofer, C., Davis, K., Evans, R., Fuentes, J., Goldstein, A., Katul, G., Law, B., Lee, X.H., Malhi, Y., Meyers, T., Munger, W., Oechel, W.U.K.T.P., Pilegaard, K., Schmid, H.P., Valentini, R., Verma, S., Vesala, T., Wilson, K., Wofsy, S., 2001. FLUXNET: A new tool to study the temporal and spatial variability of ecosystem-scale carbon dioxide, water vapor, and energy flux densities. Bull. Amer. Meteorol. Soc. 82, 2415–2434.

Balsamo, G., Viterbo, P., Beijaars, A., van den Hurk, B., Hirschi, M., Betts, A.K., Scipal, K., 2009. A revised hydrology for the ECMWF model: Verification from field site to terrestrial water storage and impact in the integrated forecast system. J. Hydrometeorol. 10, 623–643.

Bengtsson, L., 2010. The global atmospheric water cycle. Environ. Res. Lett. 5, http://dx.doi.org/10.1088/1748-9326/5/2/025002.

Bennartz, R., Fischer, J., 2001. Retrieval of columnar water vapour over land from backscattered solar radiation using the Medium Resolution Imaging Spectrometer. Remote Sens. Environ. 78, 274–283.

Bishop, J.K., Rossow, W.B., 1991. Spatial and temporal variability of global surface solar irradiance. J. Geophys. Res. 96, 1839–16858.

Bowen, I.S., 1926. The ratio of heat losses by conduction and by evaporation from any water surface. Phys. Rev. 27, 779–787.

Brutsaert, W., 1999. Aspects of bulk atmospheric boundary layer similarity under free-convective conditions. Rev. Geophys., 37.

Chen, X., Su, Z., Ma, Y., Yang, K., Wen, J., Zhang, Y., 2012a. An improvement of roughness height parameterization of the Surface Energy Balance System (SEBS) over the Tibetan Plateau. J. Appl. Meteorol. Clim. 52 (3), 607–622.

Chen, X., Su, Z., Ma, Y., Yang, K., Wang, B., 2012b. Estimation of surface energy fluxes under complex terrain of Mt. Qomolangma over the Tibetan Plateau. Hydrol. Earth Syst. Sci. 17 (4), 1607–1618.

CEOS, 2009. The Earth Observation Handbook, www.eohandbook.com

de Jeu, R.A.M., Wagner, W., Holmes, T.R.H., Dolman, A.J., van de Giesen, N.C., Friesen, J., 2008. Global Soil Moisture Patterns Observed by Space Borne Microwave Radiometers and Scatterometers. Surv. Geophys. 29 (4–5), 399–420.

Dee, D.P., Uppala, S.M., Simmons, A.J., Berrisford, P., Poli, P., Kobayashi, S., Andrae, U., Balmaseda, M.A., Balsamo, G., Bauer, P., Bechtold, P., Beljaars, A.C.M., van de Berg, L., Bidlot, J., Bormann, N., Delsol, C., Dragani, R., Fuentes, M., Geer, A.J., Haimberger, L., Healy, S.B., Hersbach, H., Hólm, E.V., Isaksen, L., Kållberg, P., Köhler, M., Matricardi, M., McNally, A.P., Monge-Sanz, B.M., Morcrette, J.-J., Park, B.-K., Peubey, C., de Rosnay, P., Tavolato, C., Thépaut, J.-N., Vitart, F., 2011. The ERA-Interim reanalysis: configuration and performance of the data assimilation system. Q. J. R. Meteorol. Soc. 137, 553–597, http://dx.doi.org/10.1002/qj.828.

Deneke, H.M., Roebeling, R.A., 2010. Downscaling of METEOSAT SEVIRI 0.6 and 0.8 μm channel radiances utilizing the high-resolution visible channel. Atmos. Chem. Phys. 10, 9761–9772, http://dx.doi.org/10.5194/acp-10-9761-2010.

Deneke, H.M., Feijt, A.J., Roebeling, R.A., 2008. Estimating surface solar irradiance from METEOSAT SEVIRI-derived cloud properties. Remote Sens. Environ. 112, 3131–3141, http://dx.doi.org/10.1016/j.rse.2008.03.012.

Derrien, M., LeGléau, H., 2005. MSG/SEVIRI cloud mask and type from SAFNWC. Int. J. Remote Sens. 26, 4707–4732.

Dorigo, W., Scipal, K., Parinussa, R., Liu, Y.Y., Wagner, W., De Jeu, R., Naeimi, V., 2010. Error characterization of global active and passive microwave soil moisture data sets. Hydrol. Earth System Sci. 14, 2605–2616, http://dx.doi.org/10.5194/hess-14-2605-2010.

Entekhabi, D., Njoku, E.G., O'Neill, P.E., Kellog, K.H., Crow, W.T., Edelstein, W.N., Entin, J.K., Goodman, S.D., Jackson, T.J., Johnson, J., Kimball, J., Piepmeier, J.R., Koster, R., Martin, N., McDonald, K.C., Moghaddam, M., Moran, S., Reichle, R., Shi, J.C., Spencer, M.W., Thurman, S.W., Tsang, L., Van Zyl, J., 2010. The Soil Moisture Active Passive (SMAP) mission. Proc. IEEE 98, 704–716.

ESA, 2004. EarthCARE –Earth Clouds, Aerosols and Radiation Explorer. ESA, pp. 66, http://esamultimedia.esa.int/docs/SP_1279_1_EarthCARE.pdf, SP-1279(1).

ESA, 2006. The Changing Earth. ESA, pp. 85, http://esamultimedia.esa.int/docs/SP-1304.pdf, SP-1304.

EUMETSAT, 2010. Satellite Application Facility on Nowcasting and Very Short Range Forecasting. In: Algorithm Theoretical Basis Document for PGE13 "SEVIRI Physical Retrieval Product" (SPhR) v0.1.

Ferguson, C.R., Sheffield, J., Wood, E.F., Gao, H., 2010. Quantifying uncertainty in a remote sensing-based estimate of evapotranspiration over continental USA. Int. J. Remote Sens. 31 (14), 3821–3865.

Fischer, J., Bennartz, R., 1997. MERIS Algorithm Theoretical Basis Document (ATBD 2.4). In: Retrieval of Total Water Vapour Content from MERIS Measurements.

Fisher, J.B., Tu, K., Baldocchi, D.D., 2008. Global estimates of the land-atmosphere water flux based on monthly AVHRR and ISLSCP-II data, validated at 16 FLUXNET sites. Remote Sens. Environ. 112 (3), 901–919.

Fisher, J.B., Whittaker, R., Malhi, Y., 2011. ET come home: potential evapotranspiration in geographical ecology. Global Ecol. Biogeog. 20, 1–18.

Flerchinger, G.N., Xaio, W., Marks, D., Sauer, T.J., Yu, Q., 2009. Comparison of algorithms for incoming atmospheric long-wave radiation. Water Resour. Res. 45, W03423.

Gao, H., Tang, Q., Ferguson, C.R., Wood, E.F., Lettenmaier, D.P., 2010. Estimating the water budget of major US river basins via remote sensing. Int. J. Remote Sens. 31 (14), 3955–3978.

GCOS, 2010. Implementation plan for the Global Observing System for climate in support of the UNFCC (2010 Update), GCOS-138., pp. 180, http://www.wmo.int/pages/prog/gcos/Publications/gcos-138.pdf

GEO, 2005. GEOSS. 10-Year Implementation Plan. Reference Document, GEO 1000R , p. 73.

GEO, 2007. The full picture. http://www.earthobservations.org/documents/the_full_picture.pdf

Ghilain, N., Arboeda, A., Gellens-Meulenberghs, F., 2011. Evapotranspiration modelling at large scale using near-real time MSG SEVIRI derived data. Hydrol. Earth Syst. Sci. 15, 771–786.

Glenn, E.P., Huete, A.R., Nagler, P.L., Hirschboeck, K.K., Brown, P., 2007. Integrating remote sensing and ground methods to estimate evapotranspiration. Critical Rev. Plant Sci. 26, 139–168.

Goovaerts, P., 2000. Geostatistical approaches for incorporating elevation into the spatial interpolation of rainfall. J. Hydrol. 228, 113–129.

Held, I., Soden, B., 2000. Water vapor feedback and global warming. Annu. Rev. Energ. Environ. t 25, 441–475.

Hollweg, H.-D., 2005. Analysis of historical water vapour data. In: Visiting Scientist report of the EUMETSAT Satellite Application Facility on Climate Monitoring, 519 pp., www.cmsaf.eu

Huffman, G.J., Adler, R.F., Morrissey, M.M., Bolvin, D.T., Curtis, S., Joyce, R.J., McGavock, B., Susskind, J., 2001. Global precipitation at one-degree daily resolution from multisatellite observations. J. Hydrometeorol. 2, 36–50.

IPCC, 2008. Technical Paper on climate change and water. In: Intergovernmental Panel on Climate Change.

Jacobowitz, H., Stowe, L.L., Ohring, G., Heidinger, A., Knapp, K., Nalli, N.R., 2003. The Advanced Very High Resolution Radiometer Pathfinder Atmosphere (PATMOS) climate dataset: a resource for climate research. Bull. Amer. Meteorol. Soc. 84, 785–793, http://dx.doi.org/10.1175/BAMS-84-6-785.

Jia, Z., Liu, S., Xu, Z., Chen, Y., Zhu, M., 2012. Validation of remotely sensed evapotranspiration over the Hai River Basin, China. J. Geophys. Res. 117, D13113.

Jiménez, C., Prigent, C., Aires, F., 2009. Toward an estimation of global land surface heat fluxes from multisatellite observations. J. Geophys. Res. 114, D06305, http://dx.doi.org/10.1029/2008JD011392.

Jiménez, C., Prigent, C., Mueller, B., Seneviratne, S.I., McCabe, M.F., Wood, E.F., Rossow, W.B., Balsamo, G., Betts, A.K., Dirmeyer, P.A., Fisher, J.B., Jung, M., Kanamitsu, M., Reichle, R.H., Reichstein, M., Rodell, M., Sheffield, J., Tu, K., Wang, K., 2011. Global intercomparison of 12 land surface heat flux estimates. J. Geophys. Res. 116, D02102.

Joyce, R.J., Janowiak, J.E., Arkin, P.A., Xie, P., 2004. CMORPH: A method that produces global precipitation estimates from passive microwave and infrared data at high spatial and temporal resolution. J. Hydrometeorol. 5, 487–503.

Jung, M., Reichstein, M., Bondeau, A., 2009. Towards global empirical upscaling of FLUXNET eddy covariance observations: validation of a model tree ensemble approach using a biosphere model. Biogeoscience 6, 2001–2013.

Jung, M., Reichstein, M., Ciais, P., Seneviratne, S.I., Sheffield, J., Goulden, M.L., Bonan, G., Cescatti, A., Chen, J., de Jeu, R., Dolman, A.J., Eugster, W., Gerten, D., Gianelle, D., Gobron, N., Heinke, J., Kimball, J., Law, B.E., Montagnani, L., Mu, Q., Mueller, B., Oleson, K., Papale, D., Richardson, A.D., Roupsard, O., Running, S., Tomelleri, E., Viovy, N., Weber, U., Williams, C., Wood, E., Zaehle, S., Zhang, K., 2010. Recent decline in the global land evapotranspiration trend due to limited moisture supply. Nature 467, 951–954.

Kalma, J.D., McVicar, T.R., McCabe, M.F., 2008. Estimating land surface evaporation: a review of methods using remotely sensed surface temperature data. Surv. Geophys. 29, 421–469.

Kerr, Y., Waldteufel, P., Wigneron, J.-P., Delwart, S., Cabot, F., Boutin, J., Escorihuela, M.-J., Font, J., Reul, N., Gruhier, C., Juglea, S.E., Drinkwater, M.R., Hahne, A., Martin-Neira, M., Mecklenburg, S., 2010. The SMOS mission: New tool for monitoring key elements of the global water cycle. Proc. IEEE 98, 666–687.

Kidd, C., Levizzani, V., 2011. Status of satellite precipitation retrievals. Hydrol. Earth Syst. Sci. 15, 1109–1116, http://dx.doi.org/10.5194/hess-15-1109-2011.

Kolmogorov, A.N., 1991. The local structure of turbulence in incompressible viscous fluid for very large Reynolds numbers. Proc. Math. Phys. Sci. 434, 9–13.

Kummerow, C., Hong, Y., Olson, W.S., Yang, S., Adler, R.F., Mccollum, J., Ferraro, R., Petty, G., Shin, D.B., Andwilheit, T.T., 2001. The evolution of the Goddard profiling algorithm (GPROF) for rainfall estimation from passive microwave sensors. J. Appl. Meteorol. 40, 1801–1820.

Kustas, W.P., Norman, J.M., 2000. A two-source energy balance approach using directional radiometric temperature observations for sparse canopy covered surfaces. Agron J. 92, 847–854.

Lanzante, J.R., Gahrs, G.E., 2000. 'Clear-sky bias' of TOVS upper-tropospheric humidity. J. Clim. 13 (22), 4034–4041.

Lenderink, G., van Meijgaard, E., 2010. Linking increases in precipitation extremes to atmospheric temperature and moisture changes. Environ. Res. Lett. 5, http://dx.doi.org/10.1088/1748-9326/5/2/025208.

Lensky, I.M., Rosenfeld, D., 2006. The time-space exchangeability of satellite retrieved relations between cloud top temperature and particle effective radius. Atmos. Chem. Phys. 6, 2887–2894.

Leuning, R., Zhang, Y.Q., Rajaud, A., Cleugh, H., Tu, K., 2008. A simple surface conductance model to estimate regional evaporation using MODIS leaf area

index and the Penman-Monteith equation. Water Resour. Res. 44, W10419, http://dx.doi.org/10.1029/2007WR006562.
Li, Z., Muller, J.P., Cross, P., 2003. Comparison of precipitable water vapor derived from radiosonde, GPS, and moderate-resolution imaging spectroradiometer measurements. J. Geophys. Res. 108 (D20), 4651, http://dx.doi.org/10.1029/2003JD003372.
Lindenbergh, R., Keshin, M., van der Marel, H., Hanssen, R., 2008. High resolution spatio-temporal water vapour mapping using GPS and MERIS observations. Int. J. Remote Sens. 29 (8), 2393–2409.
Liu, S.M., Xu, Z.W., Wang, W.Z., Jia, Z.Z., Zhu, M.J., et al., 2001. A comparison of eddy-covariance and large aperture scintillometer measurements with respect to the energy balance closure problem. Hydrol. Earth Syst. Sci. 15, 1291–1306.
Liu, Y.Y., Parinussa, R.M., Dorigo, W.A., De Jeu, R.A.M., Wagner, W., van Dijk, A.I.J.M., McCabe, M.F., Evans, J.P., 2011. Developing an improved soil moisture dataset by blending passive and active microwave satellite-based retrievals. Hydrol. Earth Syst. Sci. 15, 425–436.
Ma, Y., Kang, S., Zhu, L., Xu, B., Tian, L., Yao, T., 2008. Tibetan Observation and Research Platform- Atmosphere–land interaction over a heterogeneous landscape. Bull. Amer. Meteor. Soc. 89, 1487–1492.
Ma, Y., Zhong, L., Su, Z., Ishikawa, H., Menenti, M., et al., 2006. Determination of regional distributions and seasonal variations of land surface heat fluxes from Landsat-7 Enhanced Thematic Mapper data over the central Tibetan Plateau area. J. Geophys. Res. 111, D10305.
McCabe, M.F., Wood, E.F., 2006. Scale influences on the remote estimation of evapotranspiration using multiple satellite sensors. Remote Sens. Environ. 105, 271–285.
MERIS PQSR, 2006. MERIS Products Quality Status Report, Issue: Version 1. Prepared by the MERIS Quality Working Group.
Minnis, P., Garber, D.P., Young, D.F., Arduini, R.F., Takano, Y., 1988. Parameterizations of reflectance and effective emittance for satellite remote sensing of cloud properties. J. Atmos. Sci. 55, 3313–3339.
Miralles, D.G., Crow, W.T., Cosh, M.H., 2010. Estimating spatial sampling errors in coarse-scale soil moisture estimates derived from point-scale observations. J. Hydrometeorol. 11 (6), 1423–1429.
Miralles, D.G., Holmes, T.R.H., De Jeu, R.A.M., Gash, J.H., Meesters, A.G.C.A., Dolman, A.J., 2011. Global land-surface evaporation estimated from satellite-based observations. Hydrol. Earth Syst. Sci. 15, 453–469.
Monin, A.S., Obukhov, A.M., 1954. Basic laws of turbulent mixing I the surface layer of the atmosphere. Trudy Geofiz. Inst. AN SSSR 24 (151), 163–187, available at www.mcnaughty.com
Monteith, J.L., 1965. Evaporation and the environment. Symp. Soc. Exp. Boil., 203–234.
Mu, Q., Heinsch, F.A., Zhao, M., Running, S.W., 2007. Development of a global evapotranspiration algorithm based on MODIS and global meteorology data. Remote Sens. Environ. 111, 519–536, http://dx.doi.org/10.1016/j.rse.2007.04.015.
Mu, Q., Jones, L.A., Kimball, J.S., McDonald, K.C., Running, S.W., 2009. Satellite assesment of land surface evapotranspiration for the pan-Arctic domain. Water Resour. Res. 45, W09420, http://dx.doi.org/10.1029/2008WR007189.
Mueller, B., Seneviratne, S.I., Jimenez, C., Corti, T., Hirschi, M., Balsamo, G., Ciais, P., Dirmeyer, P.F., Guo, J.B., Jung, Z., Maignan, M., McCabe, F., Reichle, M.F., Reichstein, R.H., Rodell, M., Sheffield, M., Teuling, J., Wang, A.J., Wood, K., Zhang, E.F.Y., 2011. Evaluation of global observations-based evapotranspiration datasets and IPCC AR4 simulations. Geophys. Res. Lett. 38, http://dx.doi.org/10.1029/2010GL046230, L06402.
Müller, R., Matsoukas, C., Gratzki, A., Hollmann, R., Behr, H., 2009. The CM-SAF operational scheme for the satellite based retrieval of solar surface irradiance – a LUT based eigenvector hybrid approach. Remote Sens. Environ. 113 (5), 1012–1024.
Nakajima, T., King, M.D., 1990. Determination of the optical thickness and effective particle radius of clouds from reflected solar radiation measurements. Part I. Theory. J. Atmos. Sci. 47, 1878–1893.
Obukhov, A.M., 1971. Turbulence in an atmosphere with a non-uniform temperature. Bound. -Lay. Meteorol. 2, 7–29.
Onogi, K., Tsutsui, J., Koide, H., Sakamoto, M., Kobayashi, S., Hatsushika, H., Matsumoto, T., Yamazaki, N., Kamahori, H., Takahashi, K., Kadokura, S., Wada, K., Kato, K., Oyama, R., Ose, T., Mannoji, N., Taira, R., 2007. The JRA-25 Reanalysis. J. Meteor. Soc. Japan 85, 369–432.
Pauwels, V.R.N., Samson, R., 2006. Comparison of different methods to measure and model actual evapotranspiration rates for a wet sloping grassland. Agric. Water Manag. 82, 1–24.
Pauwels, V.R.N., Timmermans, W., Loew, A., 2008. Comparison of the estimated water and energy budgets of a large winter wheat field during AgriSAR 2006 by multiple sensors and models. J. Hydrol. 349, 425–440.
Penman, H.L., 1948. Natural evaporation from open water, bare soil and grass. Proc. Roy. Soc., A, 120–146.
Petty, G.W., 2001. Physical and Microwave Radiative Properties of Precipitating Clouds. Part II: A Parametric 1D Rain-Cloud Model for Use in Microwave Radiative Transfer Simulations. J. Appl. Meteorol. 40, 2115–2129.
Pinker, R.T., Laszlo, I., 1992. Modeling surface solar irradiance for satellite applications on global scale. J. Appl. Meteorol. 31, 194–211.
Prasad, A.K., Singh, R.P., 2009. Validation of MODIS Terra, AIRS, NCEP/DOE AMIP-II Reanalysis-2, and AERONET Sun photometer derived integrated precipitable water vapor using ground-based GPS receivers over India. J. Geophys. Res. 114, D05107, http://dx.doi.org/10.1029/2008JD011230.
Randal, D.L., Haar, T.H.V., Ringerud, M.A., Stephens, G.L., Greenwald, T.J., Combs, C.L., 1996. A new global water vapor dataset. Bull. Amer. Meteorol. Soc. 77, 1233–1246.
Rienecker, M.M., Suarez, M.J., Gelaro, R., Todling, R., Bacmeister, J., Liu, E., Bosilovich, M.G., Schubert, S.D., Takacs, L., Kim, G.K., Bloom, S., Chen, J.Y., Collins, D., Conaty, A., Da Silva, A., Gu, W., Joiner, J., Koster, R.D., Lucchesi, R., Molod, A., Owens, T., Pawson, S., Pegion, P., Redder, C.R., Reichle, R., Robertson, F.R., Ruddick, A.G., Sienkiewicz, M., Woollen, J., 2011. MERRA–NASA's modern-era retrospective analysis for research and applications. J. Climate 24 (14), 3624–3648.
Rosenfeld, D., Gutman, G., 1994. Retrieving microphysical properties near the tops of potential rain clouds by multispectral analysis of AVHRR data. Atmos. Res. 34, 259–283.
Rodell, M., Houser, P.R., Jambor, U., Gottschalck, J., Mitchell, K., Meng, C.J., Arsenault, K., Cosgrove, B., Radakovich, J., Bosilovich, M., Entin, J.K., Walker, J.P., Lohmann, D., Toll, D., 2004. The Global Land Data Assimilation System. Bull. Amer. Meteorol. Soc. 85, 381–394.
Roebeling, R.A., Holleman, I., 2009. Development and validation of rain rate retrievals from SEVIRI using weather radar observations. J. Geophys. Res. 114, D21202, http://dx.doi.org/10.1029/2009JD012102.
Roebeling, R.A., Feijt, A.J., Stammes, P., 2006. Cloud property retrievals for climate monitoring: implications of differences between SEVIRI on METEOSAT-8 and AVHRR on NOAA-17. J. Geophys. Res. 11, D20210, http://dx.doi.org/10.1029/2005JD006990.
Schulz, J., Albert, P., Behr, H.D., Caprion, D., Deneke, H., Dewitte, S., Dürr, B., Fuchs, P., Gratzki, A., Hechler, P., Hollmann, R., Johnston, S., Karlsson, K.-G., Manninen, T., Müller, R., Reuter, M., Riihel, A., Roebeling, R., Selbach, N., Tetzlaff, A., Thomas, W., Werscheck, M., Wolters, E., Zelenka, A., 2009. Operational climate monitoring from space: the EUMETSAT Satellite Application Facility on Climate Monitoring (CM-SAF). Atmos. Chem. Phys. 9, 1687–1709.
Schwärz, M., 2004. Joint Temperature, Humidity, Ozone, and Sea Surface Temperature Retrieval from Infrared Atmospheric Sounding Interferometer Data, Dissertation , University of Graz.
Sheffield, J., Wood, E.F., Munoz-Arriola, F., 2010. Long-term regional estimates of evapotranspiration for Mexico based on downscaled ISCCP data. J. Hydrometeor. 11 (2), 253–275.
Sohn, B.-J., Bennartz, R., 2008. Contribution of water vapor to observational estimates of longwave cloud radiative forcing. J. Geophys. Res. 113, http://dx.doi.org/10.1029/2008JD010053, D20107.
Stammes, P., 2001. Spectral radiance modeling in the UV-Visible range. In: Smith, W.L., Timofeyev, Y.M. (Eds.), IRS 2000: Current problems in Atmospheric Radiation. A. Deepak Publ., Hampton, VA, pp. 385–388.
Stamnes, K., Tsay, S., Wiscombe, W., Jayaweera, K., 1988. Numerically stable algorithm for discrete-ordinate-method radiative transfer in multiple scattering and emitting layered media. Appl. Optics 27, 2502–2509.
Stubenrauch, C.J., Cros, S., Lamquin, N., Armante, R., Chédin, A., Crevoisier, C., Scott, N.A., 2008. Cloud properties from atmospheric infrared sounder and evaluation with cloud-aerosol lidar and infrared pathfinder satellite observations. J. Geophys. Res. 113, D00A10, http://dx.doi.org/10.1029/2008JD009928.
Stubenrauch, C.J., Rossow, W.B., Chéruy, F., Chédin, A., Scott, N.A., 1999. Clouds as seen by satellite sounders (3I) and imagers (ISCCP). Part I: Evaluation of cloud parameters. J. Climate 12, 2189–2213.
Su, Z., 2002. The Surface Energy Balance System (SEBS) for estimation of turbulent heat fluxes. Hydrol. Earth Syst. Sci. 6, 85–99.
Su, Z., Roebeling, R.A., Schulz, J., Holleman, I., Levizzani, V., Timmermans, W.J., Rott, H., Mognard-Campbell, N., de Jeu, R., Wagner, W., Rodell, M., Salama, M.S., Parodi, G.N., Wang, L., 2011. Observation of hydrological processes using remote sensing. In: Peter Wilderer (Ed.), Treatise on Water Science, vol. 2. Academic Press, Oxford, pp. 351–399.
Su, Z., Schmugge, T., Kustas, W.P., Massman, W.J., 2001. An evaluation of two models for estimation of the roughness height for heat transfer between the land surface and the atmosphere. J. Appl. Meteorol. 40, 1933–1951.
Su, Z., Wen, Z., Wagner, W., 2010. Preface "Advances in land surface hydrological processes–field observations, modeling and data assimilation". Hydrol. Earth Syst. Sci. 14, 365–367.
Susskind, J., Piraino, P., Rokke, L., Iredell, L., Mehta, A., 1997. Characteristics of the TOVS Pathfinder Path A dataset. Bull. Amer. Meteor. Soc. 78, 1449–1472.
Timmermans, J., Su, Z., Van der Tol, C., Verhoef, A., Verhoef, W., 2013. Quantifying the uncertainty in estimates of surface–atmosphere fluxes through joint evaluation of the SEBS and SCOPE models. Hydrol. Earth Syst. Sci. 17, 1561–1573.
Todd, M.C., Barrett, E.C., Beaumont, M.J., Green, J.L., 1995. Satellite identification of rain days over the upper Nile river basin using an optimum infrared rain/no-rain threshold temperature model. J. Appl. Meteorol. 34, 2600–2611.
Trenberth, K.E., Stepaniak, D.P., 2003. Co-variability of components of poleward atmospheric energy transports on seasonal and interannual timescales. J. Clim. 16, 3690–3704.
Uppala, S.M., Kallberg, P.W., Simmons, A.J., Andrae, U., Bechtold, V.D., Fiorino, M., Gibson, J.K., Haseler, J., Hernandez, A., Kelly, G.A., Li, X., Onogi, K., Saarinen, S., Sokka, N., Allan, R.P., Andersson, E., Arpe, K., Balmaseda, M.A., Beljaars, A.C.M., Van De Berg, L., Bidlot, J., Bormann, N., Caires, S., Chevallier, F., Dethof, A., Dragosavac, M., Fisher, M., Fuentes, M., Hagemann, S., Holm, E., Hoskins, B.J., Isaksen, L., Janssen, P.A.E.M., Jenne, R., McNally, A.P., Mahfouf, J.F., Morcrette, J.J., Rayner, N.A., Saunders, R.W., Simon, P., Sterl, A., Trenberth, K.E., Untch, A., Vasiljevic, D., Viterbo, P., Woollen, J., 2005. The ERA-40 re-analysis. Quart. J. R. Meteorol. Soc. 131, 2961–3012.
Van der Kwast, J., Timmermans, W., Gieske, A., Su, Z., Olioso, A., Jia, L., Elbers, J., Karssenberg, D., de Jong, S., 2009. Evaluation of the Surface Energy Balance

System (SEBS) applied to ASTER imagery with flux-measurements at the SPARC 2004 site (Barrax, Spain). Hydrol. Earth Syst. Sci. 13 (7), 1337–1347.
van der Tol, C., van der Tol, S., Verhoef, A., Su, B., Timmermans, J., Houldcroft, C., Gieske, A., 2009a. A Bayesian approach to estimate sensible and latent heat over vegetated land surface. Hydrol. Earth Syst. Sci. 13, 749–758.
van der Tol, C., Verhoef, W., Timmermans, J., Verhoef, A., Su, Z., 2009b. An integrated model of soil-canopy spectral radiances, photosynthesis, fluorescence, temperature and energy balance. Biogeoscience 6, 3109–3129.
Verhoef, A., Campbell, C.L., 2005. Evaporation measurement, Ch. 40. In: Anderson, M.G. (Ed.), Encyclopedia of Hydrological Sciences, Vol. 1. John Wiley, Chichester, UK, pp. 589–601.
Verhoef, A., McNaughton, K.G., Jacobs, A.F.G., 1999. A parameterization of momentum roughness length and displacement height for a wide range of canopy densities. Hydrol. Earth Syst. Sci. 1, 81–91.
Verhoef, W., Jia, L., Xiao, Q., Su, Z., 2007. Unified optical-thermal four-stream radiative transfer theory for homogeneous vegetation canopies. IEEE Trans. Geosci. Remote Sens. 45, 1808–1822.
Vinukollu, R.K., Wood, E.F., Ferguson, C.R., Fisher, J.B., 2011. Global estimates of evapotranspiration for climate studies using multi-sensor remote sensing data: Evaluation of three process-based approaches. Remote Sens. Environ. 115, 801–823.
Wang, K., Dickinson, R.E., Wild, M., Liang, S., 2010a. Evidence for decadal variation in global terrestrial evapotranspiration between 1982 and 2002, 1. Model development. J. Geophys. Res. 115, D20112, http://dx.doi.org/10.1029/2009JD013671.
Wang, K., Dickinson, R.E., Wild, M., Liang, S., 2010b. Evidence for decadal variation in global terrestrial evapotranspiration between 1982 and 2002: 2. Results. J. Geophys. Res. 115, D20113, http://dx.doi.org/10.1029/2010JD013847.
Wang, K., Wang, P., Li, Z., Cribb, M., Sparrow, M., 2007. A simple method to estimate actual evapotranspiration from a combination of net radiation, vegetation index, and temperature. J. Geophys. Res. 112, D15107, http://dx.doi.org/10.1029/2006JD008351.
Wang, P., Stammes, P., Mueller, R., 2011. Surface solar irradiance from SCIAMACHY measurements: algorithm and validation, Atmos. Meas. Tech. Discuss. 4, 873–912, http://dx.doi.org/10.5194/amtd-4-873-2011.
Wang, P., Stammes, P., van der, A., Pinardi, R., van Roozendael, G.M., 2008. FRESCO+: an improved O2 A-band cloud retrieval algorithm for tropospheric trace gas retrievals. Atmos. Chem. Phys. 8, 6565–6576, http://dx.doi.org/10.5194/acp-8-6565-2008.
Wang, S., Zhang, Y., Lv, S., Liu, H., Shang, L., 2013. Estimation of turbulent fluxes using the flux-variance method over alpine meadows surface in eastern Tibetan Plateau. Adv. Atmos. Sci. 30 (2), 411–424.
Wentz, F.J., 1997. A well-calibrated ocean algorithm for special sensor microwave/imager. J. Geophys. Res. 102, 8703–8718.
Wentz, F.F., Spencer, R.W., 1998. SSM/I rain retrievals within a unified all-weather ocean algorithm. J. Atmos. Sci. 55, 1613–1627.
WMO/GCOS, 2006. Systematic Observation Requirements for Satellite-based Products for Climate – Supplemental details to the satellite-based component of the Implementation Plan for the Global Observing System for Climate in Support of the UNFCCC (GCOS-107, WMO/TD. No 1338, September 2006).
WMO/ReqObs, 2001. Requirements for observations for global NWP. WMO, Expert team on observational data requirements and redesign of the global observing system, Reference Number CBS/OPAG-IOS (ODRRGOS-4)/INF. 4, 11 October 2001.
Wolters, E.L.A., van den Hurk, B.J.J.M., Roebeling, R.A., 2011. Evaluation of rainfall retrievals from SEVIRI reflectances over West Africa using TRMM-PR and CMORPH. Hydrol. Earth Syst. Sci. 15, 437–451, http://dx.doi.org/10.5194/hess-15-437-2011.
Zhang, Y., Rossow, W.B., Lacis, A.A., Oinas, V., Mishchenko, M.I., 2004. Calculation of radiative fluxes from the surface to top of atmosphere based on ISCCP and other global data sets: Refinements of the radiative transfer model and the input data. J. Geophys. Res. 109, http://dx.doi.org/10.1029/2003JD004457, D19105.
Zhang, L., Li, Y., Li, Y., Zhao, X., 2012. Seasonal changes of turbulent fluxes at a typical agricultural site in the Chengdu Plain based on quality-controlled data. J. Meteorol. Soc. Japan. Ser. II 90C, 195–202.
Zhang, K., Kimball, J.S., Mu, Q., Jones, L.A., Goetz, S.J., Running, S.W., 2009. Satellite based analysis of northern ET trends and associated changes in the regional water balance from 1983 to 2005. J. Hydrol. 379, 92–110.
Zhang, K., Kimball, J.S., Nemani, R.R., Running, S.W., 2010a. A continuous satellite-derived global record of land surface evapotranspiration from 1983-2006. Water Resour. Res., http://dx.doi.org/10.1029/2009WR008800.
Zhang, L., Potter, N., Zhang, Y., 2010b. Correction to "Water balance modeling over variable time scales based on the Budyko framework – Model development and testing". J. Hydrol. 390 (1–2), 121–122, http://dx.doi.org/10.1016/j.jhydrol.2010.05.027 [J. Hydrol. 360 (2008) 117–131. http://dx.doi.org/10.1016/j.jhydrol.2008.07.021].
Zhang, Y.Q., Leuning, R., Hutley, L.B., Beringer, J., McHugh, I., Walker, J.P., 2010c. Using long-term water balances to parameterize surface conductances and calculate evaporation at 0.05 degrees spatial resolution. Water Resour. Res. 46, http://dx.doi.org/10.1029/2009WR008716, W05, 512.